DETERMINATION OF RHEOLOGICAL DATA OF SILICA SUSPENSIONS WITH A CAPILLARY VISCOMETER

by 2214

DAVID F. CALA

B. S. (Chem. Eng.), Universidad Industrial de Santander, 1968
M. S. (Mathematics), Kansas State Teachers College, 1969

A MASTER'S THESIS

submitted in partial fulfillment of the

requirements for the degree

MASTER OF SCIENCE

Department of Chemical Engineering

KANSAS STATE UNIVERSITY
Manhattan, Kansas

1971

Approved by:

Walter P. Walawender
Major Professor

TABLE OF CONTENTS

ILLEGIBLE DOCUMENT

THE FOLLOWING DOCUMENT(S) IS OF POOR LEGIBILITY IN THE ORIGINAL

THIS IS THE BEST COPY AVAILABLE

LIST OF TABLES

LIST OF FIGURES

Figure Page

THIS BOOK CONTAINS NUMEROUS PAGES WITH THE ORIGINAL PRINTING BEING SKEWED DIFFERENTLY FROM THE TOP OF THE PAGE TO THE BOTTOM.

THIS IS AS RECEIVED FROM THE CUSTOMER.

CHAPTER 1

INTRODUCTION

Interest in the flow properties of concentrated suspensions has increased in the last few years. It is important not only from the point of view of basic research but also for design applications to several current industrial processes. Also, silica suspensions may be a suitable test fluid for model blood flow experiments. The flow of blood has been the subject of a considerable amount of research. Some of these studies will be briefly presented in Chapter 2.

A basic understanding of the rheological behavior of concentrated suspensions is important to manufacturing processes in which large volumes of concentrated suspensions are handled. It is also important in the hydraulic transportation of solids by pipelines and for the design of pipelines where such materials are transported (13).

Some of the industries where this type of transportation has been used are the following:

The coal industry, in which slurried coal has been transported with success in several places of the world (39, 48).

Other materials such as iron concentrates (24), limestone (47), metal ores (18), phosphates and fertilizers, can be economically transported as slurries. Application of slurry transportation is also important in the slurry-fueled nuclear reactors (49). Another important application of slurry transportation is the transport of solid wastes (18).

Many researches have worked in the field of rheology of suspensions. A brief review of some important studies in this field will be considered in

Chapter 2. Most of these studies have been carried out using rotational viscometers. The approach in this study was to employ a modified form of the capillary viscometer of Benis (2) to examine the rheological behavior of suspensions. This viscometer has the features of being (1) low cost and (2) easy to operate. A detailed description of the apparatus will be considered in Chapter 4.

Since most suspensions behave as non-Newtonian fluids, some general considerations concerning this field will follow.

1.1 General Considerations of Non-Newtonian Fluids

Consider a thin layer of fluid between two parallel planes a distance dy apart as in Figure 1. A shearing force F is applied to one of the plates, the other being maintained fixed. At steady state, the force F will be balanced by an internal force in the fluid due to its viscosity. A Newtonian fluid is defined as one for which the shear stress, τ_{yx}, or the force per unit area, is directly proportional to the velocity gradient.

$$\frac{F}{A} = \tau_{yx} \propto \frac{du}{dy} = \mu\left(-\frac{du}{dy}\right) = \mu\,\gamma, \qquad (1.1\text{-}1)$$

The proportionality constant μ is the viscosity of the fluid, $\frac{du}{dy}$ is the velocity gradient or commonly called the shear rate γ.

The Newtonian viscosity μ, depends only on temperature and pressure and is independent of the rate of shear. The diagram relating shear stress and rate of shear for Newtonian fluids (called "flow curve"), is therefore a straight line passing through the origin and having a slope μ.

Fluids for which the flow curve (τ vs γ) is not linear or does not pass through the origin or both for a given temperature and pressure are called non-Newtonian.

THIS BOOK CONTAINS NUMEROUS PAGES WITH DIAGRAMS THAT ARE CROOKED COMPARED TO THE REST OF THE INFORMATION ON THE PAGE.

THIS IS AS RECEIVED FROM CUSTOMER.

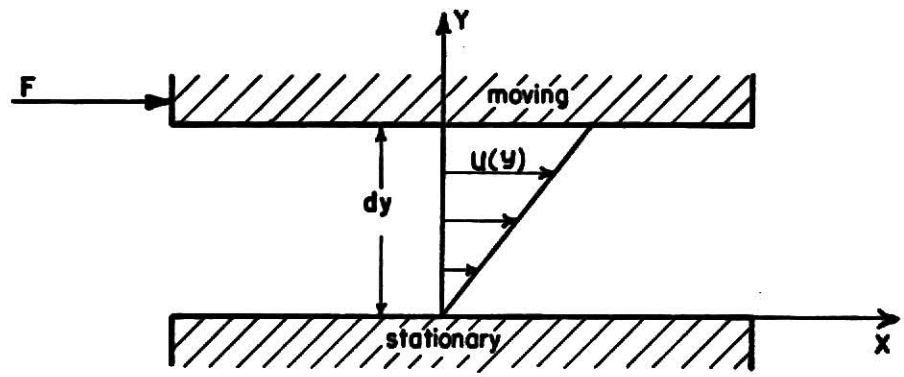

Fig. 1. Steady laminar flow of a fluid contained between two parallel planes.

Non-Newtonian fluids are classified into three broad groups as follows (3, 40, 51):

1. Time independent fluids. These fluids are those in which the rate of shear at a given point is solely dependent upon the instantaneous shear stress at that point.

2. Time-dependent fluids. These fluids are those in which the shear rate is a function of both the magnitude and the duration of shear and possibly of the time lapse between consecutive applications of shear stress.

3. Viscoelastic fluids. These are fluids that show partial elastic recovery upon the removal of a deforming shear stress.

Since most suspensions can be classified as time-independent non-Newtonian fluids a brief review of this group follows.

Fluids of this type are described by a rheological equation obtained by simplifying the constitutive equation for the hypothetical Stokesian fluid. This equation is given below.

$$\gamma = f(\tau). \qquad (1.1\text{-}2)$$

The details concerning this equation are given in Chapter 3. This equation states that the rate of shear at any point in the fluid is a simple function of the shear stress at that point. Sometimes, these fluids are referred to as "non-Newtonian viscous fluids." The rheological models of this type which were of direct concern to the present investigation will be considered in Chapter 3.

Time-independent fluids can be further classified into those which exhibit a yield stress and those which do not.

a) Fluids with a Yield Stress: A substance that belongs to this category has the property of remaining rigid when the applied shear stress is of a

smaller magnitude than the yield stress τ_y, but flows when the shear stress exceeds τ_y. The physical explanation of this behavior is that the fluid at rest contains an internal three dimensional structure which is capable of preventing movement for values of shear stress less than the yield value. For a stress greater than τ_y the internal structure breaks down, allowing fluid to move.

Some of the mathematical models describing this class of fluids are presented in detail, by Skelland (40). Typical flow curves for fluids with and without a yield stress are shown in Figure 2.

b) Fluids without a yield stress: The flow curves for these fluids pass through the origin and are divided in two categories, pseudo plastic and dilatant fluids. Most non-Newtonian fluids without a yield stress are pseudo plastic. The flow curves of these materials are characterized by linearity at very low and very high shear rates. The apparent viscosity of these materials decreases progressively with increasing shear rate. A logarithmic plot of τ_{yx} versus γ is often observed to be linear over a wide range of shear rate. The physical interpretation of this phenomenon is that with increasing shear rates the particles or molecules are progressively aligned. Instead of the random intermingled state which exists when the fluid is at rest, the major axes are brought into line with the direction of flow. The apparent viscosity decreases with increasing shear rate until no further alignment along the streamlines if possible and the flow curve then becomes linear.

Some of the mathematical models for this class of fluids are presented by Skelland (40).

With dilatant fluids, the apparent viscosity increases with increasing

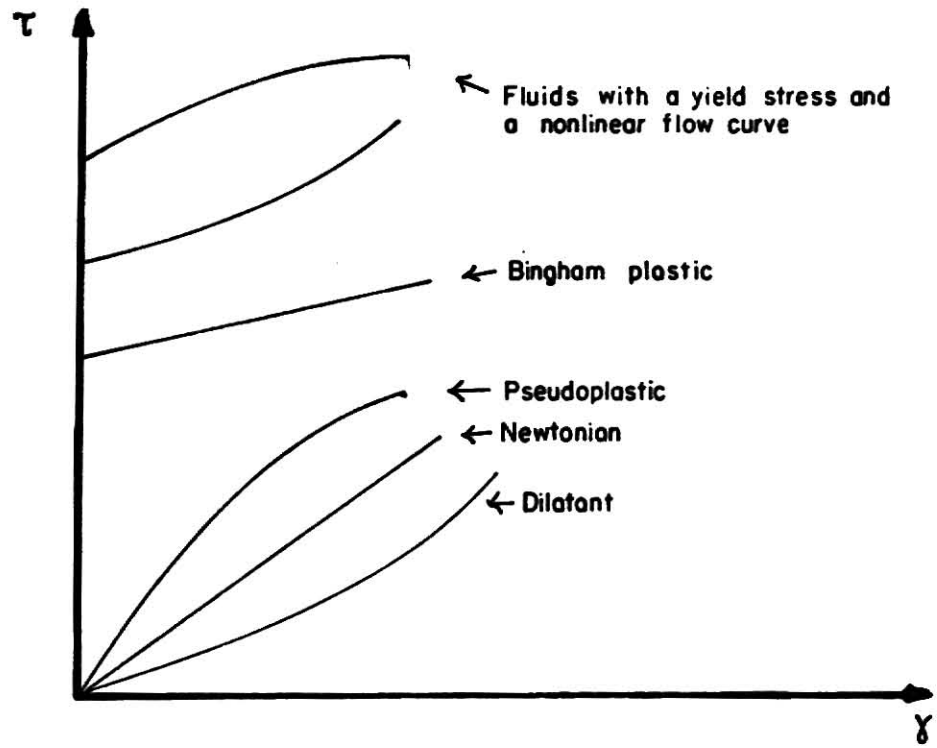

Fig. 2. Typical flow curves for time-independent non- Newtonian fluids.

shear rate. The physical explanation of this behavior can be given in the following terms; at low rates of shear, the liquid lubricates the motion of one particle past another and the stresses are consequently small. At higher rates of shear, the initial structure is broken up and the material expands providing an increase in the voids between particles. In this situation there is insufficient liquid in the new structure to lubricate the particles as they flow past each other and the applied stresses have to be much greater. The behavior results in an increase in the apparent viscosity with increasing rates of shear.

Typical flow curves for dilatant fluids are also included in Figure 2.

1.2 Objectives

The main objectives of the present investigation were; (1) to obtain rheological data for silica suspensions, with a capillary viscometer, and (2) to fit the data to a model or models which described the flow curves.

Secondary objectives of this investigation were; (1) the formulation of a pressure flow relation for a Casson fluid (which can describe flow curves for silica suspensions), (2) the development of a friction factor correlation for Casson fluids and (3) the investigation of some approximations to the Casson model.

1.3 Organization of the Thesis

A brief review of some representative studies concerned with the rheology of suspensions, and the instruments and methods employed in the evaluation of flow properties are considered in Chapter 2.

A theoretical analysis of the viscometer and methods of data analysis are presented in Chapter 3. Also some pressure flow relations and friction factor correlations are considered.

A detailed description of the instrument, the methods of calibration and the experimental procedures, are presented in Chapter 4. This is followed, in Chapter 5, by a description of the data analysis and the results obtained. Some conclusions, discussion and recommendations are presented in Chapter 6.

CHAPTER 2

LITERATURE SURVEY

A brief review of some representative studies on the rheology of suspensions, the instruments and methods employed in the evaluation of flow properties of suspensions and methods for correlating friction factor data will be presented in this chapter.

The rheological studies of suspensions can be divided in three main groups as follows:

1. The first group corresponds to those studies in which the viscosity is related to the concentration and other properties of the suspensions by means of theoretical or empirical methods. No shear dependence is considered here, and hence the suspension is treated as a Newtonian fluid.

2. The second group corresponds to those studies in which the suspensions are considered as homogeneous fluids. Shear dependence is taken into account and the constitutive equations for homogeneous non-Newtonian fluids are applied to describe the rheological behavior of the suspensions. The coefficients in these expressions must be evaluated experimentally and no attempt is made to relate them to the concentration and other properties of the suspension.

3. The third group is a combination of the above two approaches. In this case, semi-theoretical expressions have been developed which relates the shear stress and the shear rate. These expressions contain parameters which are dependent on the concentration and other properties of the suspension, and can be, at least partially, expressed in terms of basic properties. The complete evaluation of these parameters usually requires experimental data.

A wide list of references concerning the work done on disperse systems is given by Mill (29) and Scott Blair (38). Also an extensive review has been presented by Gay (12). Some representative studies corresponding to each of the above groups will follow:

Group 1

The first theoretical equation describing the viscosity of suspensions was formulated by Einstein, who obtained the following equation for very dilute suspensions of non-interacting small rigid spheres. This equation, stated below, has been discussed by a number of authors including Frisch and Simha (10):

$$\eta_{rel} = \frac{\mu}{\mu_o} = 1 + 2.5\ \phi \qquad (2.1)$$

where

η_{rel} is the relative viscosity

μ is the absolute viscosity of the suspension (poise)

μ_o is the absolute viscosity of the suspending medium (poise)

and ϕ is the volume fraction occupied by the solids.

Equation (2.1) is frequently written in terms of the specific viscosity ($\eta_{sp} = \eta_{rel} - 1$) as $\eta_{sp} = 2.5\ \phi$.

Since the Einstein equation is generally applicable only to dilute suspensions (with a few exceptions), many attempts have been made to extend this approach to higher concentrations. Scott Blair (37) has pointed out that more than fifty modifications of the Einstein equation have been proposed.

Hatschek, as discussed by Scott Blair, has proposed an equation applicable to high solid concentrations of the form

$$\eta_{rel} = \frac{1}{1 - \sqrt[3]{\phi K}} \tag{2.2}$$

where K was called the voluminosity factor. "Voluminosity" implies that some of the continuous phase is attached to the dispersed particles, thus increasing their volume.

Two other equations discussed by Scott Blair are the Arrhenius and the Guth equations. Arrhenius has proposed an equation in $\ell n(\eta)$ that is linear in C (the concentration in weight per unit volume). This equation provides a good representation of the data for many systems if they are free of electrolytes. Guth has expanded the Einstein equation in a power series in C,

$$\eta_{sp} = A\,C + BC^2 + \ldots\ldots \tag{2.3}$$

Here C is used in place of ϕ. It has been pointed out that the first two terms are often sufficient to describe a variety of data. If the above equation is divided by C the following expression results:

$$\frac{\eta_{sp}}{C} = [\eta] = A + BC, \tag{2.4}$$

where $[\eta]$ is called the reduced viscosity. Plots of reduced viscosity against C will often be straight lines for regions of low concentrations and may be extrapolated to zero concentration to evaluate the value of A. The parameter A is a generalization of the factor 2.5 in the Einstein equation.

Vand (44), has developed a theoretical equation which accounts for collision effects. This equation is given below:

$$\eta_{rel} = 1 + 2.5\,\phi + 7.349\,\phi^2 + \ldots\ldots \tag{2.5}$$

Experimental data for spherical particles obtained with Ostwald and

Couette viscometers are in good agreement with the above equation.

Robinson (10) has considered the "free volume" of liquid through which the particles can pass each other and proposed that this "free volume" is less than the actual volume due to immobilization of the solvent between the suspended particles. The following relation was proposed to account for this.

$$\eta_{rel} = \frac{k\,\phi}{1 - s'\,\phi} , \tag{2.6}$$

here s' is the relative sediment volume, defined as the volume which the sediment will occupy when the particles themselves occupy unit volume. The coefficient k is a frictional coefficient dependent on the shape, surface roughness, etc. of the particle.

Mooney (32), using a functional method, has derived an equation which described a suspension of finite concentration and accounts for interaction effects between the particles. This equation is

$$\eta_{rel} = \exp\left(\frac{2.5\,\phi}{1 - k\,\phi}\right) , \tag{2.7}$$

where k is a constant (the self-crowding factor) which can only be approximately predicted by theory.

Ting and Luebbers (43) have proposed the following relation for suspensions of glass spheres in a liquid medium of nearly equal density:

$$\eta_{rel} = \left(1 + \frac{\phi}{\phi_\infty - \phi}\right) , \tag{2.8}$$

where ϕ_∞ is the volume fraction of solids required for infinite viscosity of the suspension.

Ford (9) presents a number of theoretical and empirical relationships

for the viscosities of suspensions of spheres. He has suggested that these relationships are closer to experimental data when they are written in terms of fluidities, that is the inverse of the viscosity.

Moreland (34) has studied suspensions of coal particles in mineral oils, using a Brookfield viscometer. He has shown that the Einstein equation or modifications thereof represent the data closely for volume concentrations of less than 30 per cent. However no empirical equation was reported for higher concentrations.

Thomas (42) has proposed the following equations for dilute and concentrated suspensions respectively:

$$\eta_{rel} = 1 + 2.5\ \phi + 10.05\ \phi^2 + 0.062\ \exp\left(\frac{1.875\ \phi}{1 - 1.595\ \phi}\right) \qquad (2.9)$$

and

$$\eta_{rel} = 1 + \left(\frac{54}{5f^3}\right)\left[\frac{\phi^2}{(1 - \phi/\phi_\infty)}\right] , \qquad (2.10)$$

where f is a dimensionless factor which varies between 1 and 2 for the entire range of solids concentration.

Thomas tested the above equations with a collection of data from the literature. These data scattered about ±20% at $\phi = 0.20$ to about ±75% at $\phi = 0.50$ for Equation (2.9).

Group 2

The approach followed in the present investigation is considered in this group. Some studies of suspensions concerned with the homogeneous approach will be considered here.

Several investigators in the field of blood rheology have considered blood as a homogeneous fluid (7, 17). Most of the experimenters have concluded that blood can be described as a Newtonian fluid under conditions of

high shear and a non-Newtonian fluid at lower shear rates. The non-Newtonian region can be described by both Power law model and the Casson model over limited ranges of shear. Whitmore (50) and Scott Blair (37) discuss some of the major studies that have been conducted in this field. An extensive list of references may be found in the above mentioned sources.

Merril and coworkers (25) have investigated blood flow in hollow fibers of varying diameter. The suspensions were also tested in a rotational viscometer. For purposes of analysis of the experimental data it was assumed that blood acts as a homogeneous medium and that it obeys the empirical Casson equation:

$$\tau^{1/2} = \tau_y^{1/2} + S\,\gamma^{1/2}, \qquad (2\text{-}11)$$

where τ_y is the apparent yield stress and S is a constant. This equation was found to give an excellent fit to the shear stress-shear rate data.

In different paper, the same author (26) found non-Newtonian and Newtonian behavior at low and high shear rates respectively. The non-Newtonian data indicated a yield stress and were well represented by the empirical Equation (2-11).

Hershey and Cho (15) have studied the flow characteristics of human blood in rigid tubes. They have shown that Power law model describes the data under some flow conditions.

Tamamushi (41) has made some comparisons between Bingham plastic and Casson models for the rheological description of blood data, and has suggested that Bingham model can describe the rheological data over a limited range of shear. However it was also shown that the Casson model has a wider range of applicability.

Other important contributions to the study of non-Newtonian flow properties of blood were made by Cerny and coworkers (6) who studied blood flow in a capillary viscometer over a wide range of shearing stresses.

Benis (2), using a capillary viscometer, has tested samples of blood with hematocrits of 40 and 60, at low shear rate. The Casson model provided a good description of the data.

Mishra (30, 31) has conducted a study of the flow properties of suspensions of silica and lignite. Viscometric data for these suspensions were analyzed as a function of shear rate, and the effects of concentration and electrophoretic mobility were examined. A rotational viscometer was employed to obtain rheological data and a Zeta-meter to determine electrophoretic movability. Mishra has found that the flow properties of these suspensions are dependent on pH of the solution. In addition it was found that the Bingham plastic model and the Power law model could describe the data. The Power law model provided a better overall description of the silica suspension data. The Bingham plastic model described the data well for lignite suspensions.

Wu (52) has analyzed the rheological data obtained by Mishra. Bingham plastic, Power law and Casson models were examined. The Casson model was found to provide the best description of the data.

Group 3

Some studies on the rheology of suspensions concerned with the combined approach will be considered here.

Gay, Nelson and Armstrong (11) have developed an equation which is applicable to high solids concentration. A theoretical investigation of the flow behavior which considered the particle-particle interaction that takes

place in a settled suspension was conducted. The method takes into account the effects of liquid viscosity, liquid and solid densities, particle size, size distribution, particle surface area, volume fraction of solids in the suspension and volume fraction of solids under maximum settling conditions.

The following expression for the apparent viscosity as a function of the shear rate and properties of the suspension was reported;

$$\eta = \eta_\infty + \frac{\eta_o - \eta_\infty}{1 + (\frac{\eta_o - \eta_\infty}{g_c B})G} . \qquad (2\text{-}12)$$

Here η is the viscosity of the suspension

η_o is the viscosity parameter at low shear rates

η_∞ is the viscosity parameter at high shear rates

g_c is the force-mass conversion factor

G is the shear rate

and B is a flow parameter which was related with the aid of dimensional analysis to the volume fraction of solids, the yield stress, the viscosity and density of the suspension, and the particle diameter.

The following expressions were employed in the evaluation of the parameters B, η_o and η_∞:

$$\frac{B}{\tau_y} = C\,\phi_m^k\,(\phi_m - \phi)^\ell\,(\frac{\mu^2}{D_p^2\,\rho_p\,\tau_y})^n , \qquad (2\text{-}13)$$

$$\eta_o = \mu(\frac{\phi_m}{\phi_m - \phi})^{2.5} , \qquad (2\text{-}14)$$

and $$\eta_\infty = \mu \exp \{[2.5 + (\frac{\phi}{\phi_m - \phi})^n] \frac{\phi}{\phi_m}\} , \qquad (2\text{-}15)$$

where: n = 0.48; this was determined from a least-squares analysis of the data.

ϕ is the volume fraction solids

ϕ_m is the maximum volume fraction solids for the system

μ is the viscosity of the suspending medium

D_p and ρ_p are the diameter and density of particles

τ_y is the yield value

C is a constant of proportionality

k, ℓ are dimensionless constants

Volume fractions of solids from 28 to 55 were employed for testing the above equations, which were found to provide a good description of the experimental data.

Casson (5) has considered that the particles in a flocculated suspension form chain-like groups as a result of the mutual attractions existing between them. These groups will not in fact be straight chains, but they are treated as long cylindrical rods. The dimensions of these chains control the viscosity of the suspension. When the suspension flows the groups are subjected to disruptive stresses, the magnitude of which depends on the shear rate and the size of a group. Consequently the equilibrium group size, and hence the viscosity, varies with the shear rate.

Considering the magnitude of the interparticle forces and disruptive stresses the following equation was developed:

$$\sqrt{\tau} = k_o + k_1\sqrt{\gamma} , \qquad (2\text{-}16a)$$

where k_o and k_1 have been called the square root of the apparent yield stress τ_y and the Casson viscosity respectively. These parameters have been defined as:

$$k_o = \frac{a\,\beta}{a\alpha - 1}\left[\frac{k_1}{\eta_o^{1/2}} - 1\right] , \tag{2-16b}$$

and

$$k_1 = \left[\frac{\eta_o}{(1 - \phi)^{a\alpha-1}}\right]^{1/2} , \tag{2-16c}$$

where η_o is the viscosity of the suspending medium

ϕ is the volume concentration

a is a constant determined by the orientation of the cylindrical rods

α and β are constants depending on the magnitude of the rod axial ratio J (length divided by radius of the cylindrical rod).

Obviously, k_o and k_1 can be determined from the intersect and slope of a $\sqrt{\tau}$ versus $\sqrt{\gamma}$ plot.

Casson obtained data with suspensions made by dispersing different pigments in thin lithographic varnish. A cone and plate viscometer was employed. Experimental data were in good agreement with the theoretical Equation (2-16a).

Oka (35) has developed a theoretical model for time-independent non-Newtonian suspensions. This was based on the assumption that bonds are formed between particles and that they are broken gradually with increase in shear stress or shear rate. On the basis of this assumption, Oka has derived a differential equation to determine the flow curve of suspensions. The starting point of his development was the following equation:

$$-\frac{dn}{n} = A \frac{1}{(\tau + \theta)^{\alpha}} d\tau \ , \qquad (2\text{-}17)$$

which represents the percentage decrement of the number of bonds by the addition of a stress increment $d\tau$. This equation is a modification of the following equation proposed by Scott Blair (37):

$$-dn = A \frac{1}{\tau} d\tau \ , \qquad (2\text{-}18)$$

where τ is the shear stress

n is the number of bonds per unit volume of the suspension at value of

$-dn$ is the number of bonds broken down per unit volume by addition of a stress increment $d\tau$ at any value of τ.

A is a proportionality constant

θ is a constant which makes the percentage decrement finite when $\tau = 0$

and α is a dimensionless constant, which is less than or equal to unity.

Since there is a single-valued relation between the shear stress τ and the shear rate γ, n can be regarded as a function of γ instead of τ, and the stress increment $d\tau$ corresponds to the shear-rate increment $d\gamma$. On the basis of this consideration, Oka has proposed the following equation:

$$-\frac{dn}{n} = B \frac{1}{(\gamma + \phi)^{\alpha}} d\gamma \ , \qquad (2\text{-}19)$$

where B and ϕ are positive constants defined in a fashion similar to that for A and θ.

The above equation is a modification of the following equation proposed

by Scott Blair (37):

$$-dn = \frac{B}{m}\frac{1}{\gamma}\,d\gamma \ , \tag{2-20}$$

where B and m are proportionality constants.

When Equations (2-17) and (2-19) are combined the following equation results:

$$\frac{d\tau}{(\tau + \theta)^{\alpha}} = k_1 \frac{d\gamma}{(\gamma + \phi)^{\alpha}} \ , \tag{2-21}$$

where $k_1 = B/A$. This equation is the fundamental equation proposed by Oka and is employed to determine the flow curves of time-independent non-Newtonian suspensions.

When Equation (2-21) is integrated for $\alpha < 1$, the following expression is obtained:

$$(\tau + \theta)^{1-\alpha} = k_o + k_1\,(\gamma + \phi)^{1-\alpha} \tag{2-22}$$

where k_o is an integration constant.

This equation has been called "generalized Casson equation." Two particular cases of Equation (2-22) are of special interest. For $\alpha = 1/2$, and considering that $\tau >> \theta$ and $\gamma >> \phi$ the above equation can be reduced to

$$\tau^{1/2} = k_o + k_1\,\gamma^{1/2} \ , \tag{2-23}$$

which is the Casson equation. For $\alpha = 0$ the following expression is obtained:

$$\tau = (k_o + k_1\,\phi - \theta) + k_1\,\gamma. \tag{2-24}$$

If the yield value is considered, that is $\tau = \tau_y$ at $\gamma = 0$ the above equation

becomes:

$$\tau = \tau_y + k_1 \gamma, \tag{2-25}$$

which is the Bingham plastic model.

Integration of Equation (2-21) for $\alpha = 1$, with the boundary conditions that $\gamma = 0$ when $\tau = 0$ gives

$$\tau = \theta \left[\left(\frac{\gamma + \phi}{\phi}\right)^{k_1} - 1\right], \tag{2-26}$$

which has been called "generalized power law." The power law equation can be obtained from the above expression by assuming either $\gamma >> \phi$ or $\gamma << \phi$. Therefore, Casson, Power law, Bingham and other models can be considered as particular cases of the equation developed by Oka.

Instruments and Methods for the Study of Suspensions

Two major types of viscometers have been employed in the study of the rheological behavior of suspensions; rotational and capillary viscometers.

Rotational viscometers allow the determination of the relation between shear stress and shear rate from torque and angular velocity measurements. These instruments are divided into a variety of categories among which are the: coaxial cylinder, rotating bob in an infinite fluid and the cone-plate viscometers.

In the coaxial cylinder viscometer the material is confined in the gap between two long vertical coaxial cylinders, one of which can be rotated at various speeds while the torque on the other is measured. The variation of torque with speed can be interpreted to give the relation between shear stress and rate of shear. The coaxial cylinder viscometer is also called "couette viscometer." A modification of this viscometer is the rotating bob

viscometer which contains only one cylinder that is rotated in a fluid of infinite extent. The cone and plate viscometer consists of a flat plate and a cone with a very obtuse angle. The apex of the cone just touches the plate and the fluid fills the narrow gap formed by the cone and plate. The latter is rotated and the torque on the cone is measured. In this instrument the sample can be subjected to nearly constant shear.

Capillary viscometers are used to measure the pressure gradient and the corresponding volumetric flow rate. From this information, relationships between wall shear stress and wall shear rate can be obtained. This type of viscometer has not been as widely used as rotational viscometers for the study of rheological properties of suspensions. However a capillary viscometer was employed in this study and it did offer some definite advantages.

Benis (2) has developed a simple and inexpensive low shear capillary viscometer for the rheological study of blood. A modification of this viscometer was employed in the present investigation and will be considered in detail in Chapter 4.

Two capillary viscometers (low and high shear), for the study of non-Newtonian flow, have been developed by Maron and coworkers (22, 23). The viscometers operate under a continuously varying pressure head and can be used to obtain flow properties of non-Newtonian fluids with accuracy at low and high shear rates.

A tube viscometer for the study of non-Newtonian fluids was described by Caraher (4). The viscometer consists primarily of a 200 ft length, 1/4 in. ID tygon tubing coiled around a cylindrical support. The liquid under test is allowed to flow through the tubing while the flow rate and associated pressure drop are measured. This viscometer is a "macro" version of the

Benis instrument and was developed several years before the Benis instrument.

A comprehensive description of the commercially available viscometers that have been employed for rheological flow measurements is given by Van Wazer and coworkers (45).

Some of the methods for the evaluation of flow curves (τ versus γ) for non-Newtonian fluids will be considered here. The details of the methods which were of direct concern with the present study will be presented in Chapter 3.

Rabinowitsch (36) and Mooney (33) independently developed an expression which relates to shear stress and the shear rate for a time-independent fluid flowing through a tube. This relation will be considered in detail in Chapter 3.

Krieger and Maron have presented, in three papers (19, 20, 21), methods for the determination of the flow curves for non-Newtonian fluids. These methods permit the evaluation of shear stresses and shear rates from data obtained with rotational and capillary viscometers. The method for capillary viscometers will be considered in Chapter 3.

Reviews of the methods available for time-independent non-Newtonian fluids can be found in the books by Wilkinson (51) and Skelland (40).

Friction Factor Correlations

Another topic of concern in the present investigation is the correlation of friction factor data for time-independent non-Newtonian suspensions.

Metzner and Reed (27, 28) presented a generalized method for correlating friction factor data in terms of a generalized Reynolds number. Their method can be used for both Newtonian and non-Newtonian fluids. The correlation has been tested with data for the flow of non-Newtonian fluids and suspensions in

pipes and it was found to be theoretically rigorous in the laminar region. Further details of this method will be considered in Chapter 3.

Hershey and Smolin (18) have employed the generalized method by Metzner and Reed to correlate blood flow data. Both the laminar and turbulent regions were investigated. The laminar region was very well described by the theoretical equation $f = 16/N_{Re}$. A transition region was observed for Reynolds numbers greater than 2,400.

Hershey and Grupta (16) have also used the generalized method to analyze the effect of tube diameter on the transition region for blood flow data.

Hedström (14) has also developed a method for correlating friction factor data in terms of a modified Reynolds number and a third parameter, for Bingham plastic fluids. This additional parameters, the Hedström number is a function of the yield stress. An analogous procedure will be employed in Chapter 3, for the evaluation of friction factors for Casson fluids.

Dodge and Metzner (8) have developed a theoretical analysis for turbulent flow of non-Newtonian fluids through smooth cylindrical tubes. Experimental data were in good agreement with the theoretical equation.

Harris and Quader (13) have recently published a general relationship for predicting pressure drops for non-Newtonian fluids and solid-liquid systems flowing in pipelines. The relation accounts for the slip phenomenon and is applicable to both laminar and turbulent flow. The same authors have pointed out that their relation has advantages over the generalized friction factor methods given by Metzner and Reed and by Dodge and Metzner. Reviews of other methods are given by Wilkinson (51).

CHAPTER 3

THEORY

The rheological models that were used in this investigation, a general description of the instrument, and the analysis of unsteady state Newtonian and non-Newtonian flow are presented in this chapter. Some pressure flow relations for Power law and Casson fluids, some approximations to the Casson equation, and friction factor versus Reynolds number relationships for non-Newtonian flow are also included in the following sections.

3.1 Rheological Models

Silica suspensions can be classified as time-independent non-Newtonian fluids in the appropriate flow range. The general rheological model employed to describe these fluids can be obtained by simplification of the general constitutive equation for the hypothetical Stokesian fluid (1). The assumptions used for this simplification are:

1. Incompressible fluid
2. Simple shear flow
3. Neglect of normal stresses effects.

With these assumptions the model for the Stokesian fluid can be simplified to

$$\tilde{\tau} = -\eta \tilde{\Delta} , \tag{3.1-1}$$

where

$\tilde{\tau}$ is the viscous tensor

$\tilde{\Delta}$ is the rate deformation tensor

η is the apparent viscosity.

For steady state laminar flow, in a cylindrical tube, with $v_r = v_\theta = 0$,

Equation (3.1-1) can be further simplified to give:

$$\tau_{rz} = \eta \left(-\frac{dv_z}{dr}\right) = \eta \gamma \qquad (3.1\text{-}2)$$

The details of this simplification are readily available (3).

For Newtonian fluids the apparent viscosity η, depends on the local pressure and temperature but not on τ or γ. For time-independent non-Newtonian fluids the apparent viscosity is in addition to a scalar function of γ. Under conditions of constant pressure and temperature, these fluids can be described by the relation:

$$\gamma = f(\tau_{rz}) \ , \qquad (3.1\text{-}3)$$

that is, the rate of shear γ at any point in the fluid depends only on the shearing stress τ_{rz} at that point. This relation is employed as the starting point by most investigators for the analysis of time-independent non-Newtonian flow.

A variety of empirical functions relating the shear rates to shear stress have been proposed, and have been summarized by Skelland (40).

The following empirical rheological models have been employed in the present study.

1. Newtonian fluid

$$\gamma = f(\tau) = \frac{\tau}{\mu} \ , \qquad (3.1\text{-}4)$$

Here μ is the absolute "Newtonian" viscosity of the fluid,

2. Power law or Ostwald-deWaele model:

$$\gamma = f(\tau) = \left(\frac{\tau}{k}\right)^{1/n} \ , \qquad (3.1\text{-}5)$$

Here n and k represent the flow behavior and consistency indices of the fluid respectively.

3. Casson model

$$\gamma = f(\tau) = \frac{1}{S^2} [\tau - 2 \sqrt{\tau_y \tau} + \tau_y] \ . \qquad (3.1\text{-}6)$$

Here S represents the slope of a plot of $\sqrt{\tau}$ versus $\sqrt{\gamma}$, (sometimes called the Casson viscosity) and τ_y is the apparent yield stress.

3.2 The Rabinowitsch and Mooney Equation

This equation, developed by Rabinowitsch (36), and independently by Mooney (33), has been widely employed to evaluate the shear rate at the tube wall for a given value of the wall shear stress in capillary viscometers.

Three assumptions are required for the development of this equation:

1. Flow is laminar, so that each particle moves in a straight line, at constant velocity, parallel to the axis of the tube.
2. The fluid is time-independent under the prevailing conditions; this means that the fluid obeys Equation (3.1-3).
3. There is no slip at the tube wall.

The volumetric flow rate through a cylindrical tube is given by the well known expression,

$$Q = \int_0^{2\pi} \int_0^R v_z \, r \, dr \, d\theta = 2 \pi \int_0^R v_z r \, dr \ . \qquad (3.2\text{-}1)$$

The volumetric flow rate (Q) and the velocity gradient can be related by integrating the above equation by parts. Integration gives:

$$Q = 2 \pi \left[v_z \int_0^R r dr - \int_0^R \frac{r^2}{2} \frac{dv_z}{dr} dr \right] \ . \qquad (3.2\text{-}2)$$

The first integral of Equation (3.2-2) vanishes because of assumption 3. Therefore:

$$Q = 2\pi \int_0^R \frac{r^2}{2} \left(-\frac{dv_z}{dr}\right) dr \ , \tag{3.2-3}$$

where $$\gamma = \left(-\frac{dv_z}{dr}\right) \ . \tag{3.2-4}$$

Substitution of Equation (3.1-3) into Equation (3.2-3) gives:

$$Q = 2\pi \int_0^R \frac{r^2}{2} f\left(\tau_{rz}\right) dr \ . \tag{3.2-5}$$

Consideration of Figure 3 shows that τ_{rz} can be expressed in terms of r with the aid of a momentum balance on a cylindrical shell of thickness Δr. This balance gives after integration:

$$\tau_{rz} = \frac{r\ \Delta P}{2L} \ . \tag{3.2-6}$$

The shear stress at the wall (r = R) is:

$$\tau_w = \frac{R\ \Delta P}{2L} \ . \tag{3.2-7}$$

Combination of Equation (3.2-6) and (3.2-7) gives:

$$\tau_{rz} = \tau_w \frac{r}{R} \ , \tag{3.2-8}$$

differentiation with respect to r gives:

$$dr = \frac{R}{\tau_w} d\left(\tau_{rz}\right) \ . \tag{3.2-9}$$

Substitution of Equations (3.2-4), (3.2-8), and (3.2-9) into Equation (3.2-3) gives on simplification:

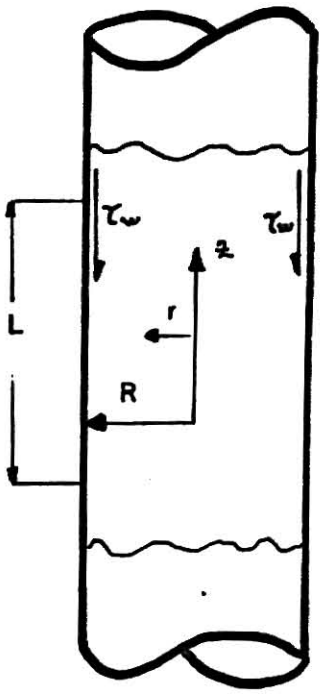

Fig. 3. Stress acting on a cylindrical fluid element of Radius R in steady flow through a vertical tube.

$$\frac{Q}{\pi R^3} = \frac{1}{\tau_w^3} \int_0^{\tau_w} \tau_{rz}^2 \, f(\tau_{rz}) \, d\tau_{rz} \, . \qquad (3.2\text{-}10)$$

The quantity $Q/\pi R^3$ can be called the reduced average velocity and has the dimensions of sec^{-1}.

From the above equation it can be seen that $Q/\pi R^3$ is a function only of τ_w. Therefore one can write:

$$\frac{Q}{\pi R^3} = F(\tau_w) = \frac{1}{\tau_w^3} \int_0^{\tau_w} \tau_{rz}^2 \, f(\tau_{rz}) d \, \tau_{rz} \qquad (3.2\text{-}11)$$

Differentiation of the above equation with respect to τ_w (with the aid of the Leibnitz Rule) gives

$$\frac{d[F(\tau_w)]}{d\tau_w} = \frac{f(\tau_w)}{\tau_w} - 3 \frac{F(\tau_w)}{\tau_w} \, , \qquad (3.2\text{-}12)$$

or

$$f(\tau_w) = 3F(\tau_w) + \tau_w \frac{d[F(\tau_w)]}{d\tau_w} \, . \qquad (3.2\text{-}13)$$

Since $F(\tau_w) = Q/\pi R^3$ and $f(\tau_w) = \gamma_w$, the above equation can be expressed as:

$$\gamma_w = (-\frac{dv_z}{dr}) = 3(\frac{Q}{\pi R^3}) + \tau_w \frac{d(Q/\pi R^3)}{d\tau_w} \, . \qquad (3.2\text{-}14)$$

This is the expression obtained by Rabinowitsch (36) and Mooney (33). It can be employed to evaluate wall shear rates from pressure drop and volumetric flow rate data. However modified forms of this equation are generally more suitable for this purpose.

3.3 Modification of Rabinowitsch Equation

Modified forms of the Rabinowitsch equation have been employed for the analysis of non-Newtonian flow data. One of the most useful is the modification of Krieger and Maron (20, 21), which is considered below.

Division of both sides of Equation (3.2-10) by τ_w give:

$$\frac{Q}{\pi R^3 \tau_w} = \frac{1}{\tau_w^4} \int_0^{\tau_w} \tau_r^2 f(\tau_r) d\tau_r , \qquad (3.3\text{-}1)$$

where the subscript z has been eliminated for simplification.

Substitution for τ_w [Equation (3.2-7)] on the LHS of Equation (3.3-1) gives

$$\frac{2L\,Q}{\pi R^4 \Delta P} = \frac{1}{\tau_w^4} \int_0^{\tau_w} \tau_r^2 f(\tau_r)\, d\tau_r \qquad (3.3\text{-}2)$$

An effective fluidity may be defined by the relation:

$$\phi_a = 8LQ/\pi R^4 \Delta P. = \frac{1}{\eta_a} , \qquad (3.3\text{-}3)$$

where η_a can be called the effective viscosity.

In the case of Newtonian fluid ϕ_a is identical with the true fluidity, which is the reciprocal of the coefficient of viscosity.

Substitution of Equation (3.3-3) into Equation (3.3-2) gives:

$$\phi_a = \frac{4}{\tau_w^4} \int_0^{\tau_w} \tau_r^2 f(\tau_r) d\tau_r . \qquad (3.3\text{-}4)$$

This equation implies that ϕ_a is independent of instrumental dimensions, a plot of ϕ_a versus τ_w for the same fluid in tubes with different dimensions should give a single curve and this is found to be the case with time

independent fluids. Differentiation of Equation (3.3-4) with respect to τ_w (with the aid of the Leibnitz Rule) gives on simplification of the result;

$$\frac{\gamma_w}{\tau_w} = \phi_a + \frac{1}{4}\frac{d\phi_a}{d\ \ell n(\tau_w)} \ . \tag{3.3-5}$$

Factoring ϕ_a from the right side of the above equation gives:

$$\frac{\gamma_w}{\tau_w} = \phi_a \left[1 + \frac{1}{4}\frac{d\ \log\ (\phi_a)}{d\ \log\ (\tau_w)}\right] \ . \tag{3.3-6}$$

Defining $\Delta F = \frac{1}{4}\frac{d\ \log\ (\phi_a)}{d\ \log\ (\tau_w)}$ in Equation (3.3-6), find: (3.3-7)

$$\frac{\gamma_w}{\tau_w} = \phi_a(1 + \Delta F) \ . \tag{3.3-8}$$

The "correction factor," ΔF ($\Delta F = 0$ for Newtonian fluids) can be calculated from the slope of a plot of $\log(\phi_a)$ vs $\log\ (\tau_w)$ plot. Equations (3.3-6) and (3.3-8) were proposed by Krieger and Maron (20, 21). The general form of Equation (3.3-8) has also been applied to concentric cylinder viscometers (19, 21). A modification of this relation was used in the analysis of the instrument employed in the present study.

3.4 Description of the Viscometer and the Analysis of Flow

A new, simple, and inexpensive low shear capillary viscometer has been recently described by Benis (2). The apparatus employed in this study is similar in construction to the above mentioned (see Chapter 4 for details). A simplified schematic diagram of the viscometer is shown in Figure 4.

The operating procedure described by Benis was different from the procedure used in this investigation. Benis suggests operation of the viscometer under quasi-steady state conditions. However, unsteady state

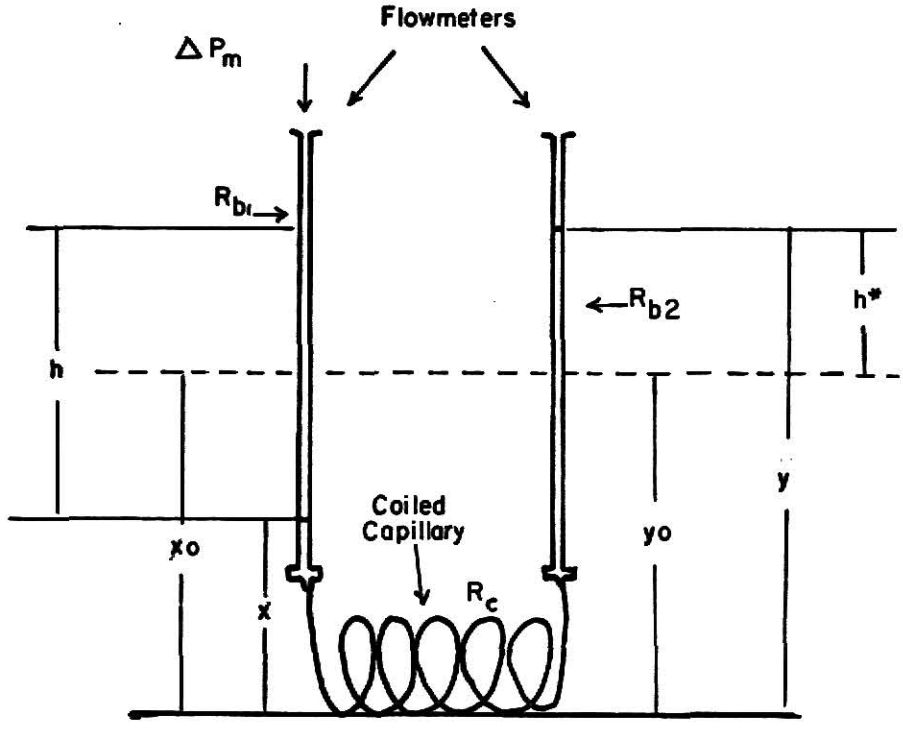

Fig. 4. Simplified schematic diagram of the viscometer.

operation appears to be more practical and can be used to advantage under certain conditions. This mode of operation was employed in the present study. The details of operation are considered in Chapter 4 and only a brief description will be given here.

With reference to Figure 4, a selected pressure ΔP_m is applied to the LHS flowmeter. As the test fluid moves through the capillary the rate of rise of the fluid in the RHS flowmeter is observed by timing the liquid meniscus at several heights (y or h^*). From these data (h^* and t) and the pressure drop (ΔP_m), the volumetric flow rate, the wall shear stress and the wall shear rate can be evaluated.

Two major simplifications were employed in the analysis and they are considered below. Because the capillary is coiled, curvature effects should be taken into consideration. However, according to the analysis of Benis for Newtonian flow, these effects are not significant and they were not considered in this investigation. In addition, Benis also showed that the time required for fully developed flow to be established was very short. This conclusion was based on Newtonian flow. The criteria of Benis (2) was applied to the instrument used in the present study and it was found that effects of developing flow could be neglected.

Maron and coworkers (22, 23) have described a capillary viscometer with continuously varying pressure head which employs mercury, or liquids of lower density, to drive the test fluids through the capillary. Their apparatus is different in construction and operation to the Benis instrument. However, their method of analysis can be applied to the Benis instrument and it will be used here to determine the relation for the actual pressure across the capillary as a function of time.

With reference to Figure 4, let x and y be the heights of the fluid in the flowmeters at any time and x_0 and y_0 the heights at equilibrium (i.e. when the pressure is the same on each side).

Define:

ΔP as the total pressure drop across the capillary,

ΔP_m as the pressure applied to the LHS flowmeter,

Rb_1 as the LHS flowmeter tube radius,

Rb_2 as the RHS flowmeter tube radius,

h^* as the meniscus height in the RHS flowmeter, relative to the equilibrium height ($h^* = y - y_0$),

h as the total difference in the column heights on each side ($h = y - x$ or $h = 2h^*$).

At any instant when the fluid is flowing through the capillary, the pressure drop ΔP across the capillary is given by

$$\Delta P = \Delta P_m + \rho g x - \rho g y \ . \tag{3.4-1}$$

When the system is in hydrostatic balance, $x = x_0$, $y = y_0$, and $\Delta P = 0$; then

$$0 = \rho g x_0 - \rho g y_0 \ . \tag{3.4-2}$$

Subtracting Equation (3.4-2) from Equation (3.4-1) gives:

$$\Delta P = \Delta P_m - \rho g[(y - y_0) - (x - x_0)] \ . \tag{3.4-2}$$

Since the volume of the fluid in the system remains constant the increase in volume on the RHS must equal the decrease in volume on the LHS, thus

$$y - y_0 = -\frac{Rb_1^2}{Rb_2^2}(x - x_0) \ . \tag{3.4-3}$$

The flowmeters used in this investigation had the same radius. For this case Equation (3.4-3) reduces to

$$y - y_0 = - (x - x_0) \ . \tag{3.4-4}$$

Substitution of this result into Equation (3.4-2) gives:

$$\Delta P = \Delta P_m - 2\rho g(y - y_0) \ . \tag{3.4-5}$$

Letting $y - y_0 = h^*$, Equation (3.4-5) can be expressed as

$$\Delta P = \Delta P_m - 2\rho g h^* \ , \tag{3.4-6}$$

or alternatively as

$$\Delta P = \Delta P_m - \rho g h \ , \tag{3.4-7}$$

where h ($h = 2h^*$) is the total difference between the fluid levels (i.e., $y - x$). The volumetric flow rate through the right hand flowmeter can be expressed as:

$$Q = \pi R_F^2 \frac{dh^*}{dt} \ , \tag{3.4-8}$$

or in terms of h

$$Q = \frac{1}{2} \pi R_F^2 \frac{dh}{dt} \ , \tag{3.4-9}$$

here R_F has been substituted for R_{b2} the radius of the flow meter tube. In case under consideration $R_F = R_{b1} = R_{b2}$.

Maron and Belner (22) have pointed out that the ratio of the capillary radius to the flowmeter radius raised to the fourth power $(R_c/R_F)^4$ should be maintained below 0.004 in order to make the resistance to flow in the flowmeter negligible compared to that in the capillary. However no theoretical

basis for this criteria was given.

For the case of Newtonian flow through the instrument, the volumetric flow rate in the capillary tube is given by the well known Poiseuille equation:

$$Q = \frac{\pi R_c^4 \Delta P}{8 \eta L} . \tag{3.4-10}$$

Substitution of Equation (3.4-7) for the pressure drop across the capillary in the above relation gives:

$$Q = \frac{\pi R_c^4 (\Delta P_m - \rho g h)}{8 \eta L} \tag{3.4-11}$$

Combining Equation (3.4-9) with Equation (3.4-11) gives on simplification:

$$\frac{dh}{(\Delta P_m - \rho g h)} = \frac{R_c^4}{4 \eta L R_F^2} dt . \tag{3.4-12}$$

The above equation can be integrated to give:

$$-\frac{1}{\rho g} \ell n (\Delta P_m - \rho g h) = \frac{R_c^4}{4 \eta L R_F^2} t + C' , \tag{3.4-13}$$

or
$$\log_{10}(\Delta P_m - \rho g h) = -\frac{B \rho}{\eta} t - c , \tag{3.4-14}$$

where
$$B = \frac{g R_c^4}{9.212 L R_F^2} \tag{3.4-15}$$

and c is a constant of integration.

From Equation (3.4-14) it follows that for a Newtonian fluid a plot of $\log(\Delta P_m - \rho g h)$ versus t should be linear. The viscosity of the fluid can be

evaluated from the slope of the line, the density of the fluid, and the instrumental dimensions.

In the present study, Equation (3.4-14) was used in the calibration of the capillary. The capillary radius (R_c) can be evaluated from the slope of a plot of $\log(\Delta P_m - \rho gh)$ versus t provided that the fluid viscosity, density, and the other geometric dimensions are known. In the calibration distilled water was employed as the fluid.

For the case of a non-Newtonian fluid, a plot of $\log(\Delta P_m - \rho gh)$ versus t may be non-linear. The $\log(\Delta P_m - \rho gh)$ versus t data can be used to evaluate the rate of shear at the wall (γ_w) as a function of the shear stress (τ_w). A method similar to that of Krieger and Maron (20) (outlined in Section 3.3) was used to obtain the relation between τ_w and γ_w. Differentiation of Equation (3.4-14) with respect to t gives:

$$\frac{d \log(\Delta P_m - \rho gh)}{dt} = - \frac{B\rho}{\eta_a} = m \ , \qquad (3.4\text{-}16)$$

where m is the slope of a plot of $\log(\Delta P_m - \rho gh)$ versus t. Since $\phi_a = 1/\eta_a$ [see Equation (3.3-3)], Equation (3.4-16) becomes:

$$\phi_a = - \frac{m}{B\rho} \ . \qquad (3.4\text{-}17)$$

The derivative appearing in Equation (3.3-7) can be evaluated for the instrument under consideration with the aid of Equations (3.2-7), (3.4-7), and (3.4-17) as follows:

$$\frac{d \log(\phi_a)}{d \log(\tau_w)} = \frac{d \ln (- \frac{m}{B\rho})}{2.303 \, d \log[\frac{R}{2L} (\Delta P_m - \rho gh)]} = \frac{\frac{dm}{m}}{2.303 \, d \log(\Delta P_m - \rho gh)} \ ;$$

since $$d \log(\Delta P_m - \rho gh) = \frac{d \log(\Delta P_m - \rho gh)}{dt} dt = m dt,$$

then, the above equation becomes:

$$\frac{d \log(\phi_a)}{d \log(\tau_w)} = \frac{1}{2.303 \, m^2} \frac{dm}{dt} . \tag{3.4-18}$$

Substitution of Equations (3.4-17) and (3.4-18) into Equation (3.3-6) gives:

$$\gamma_w = - \frac{\tau_w \, m}{B\rho} \cdot \left[1 + \frac{1}{9.212 \, m^2} \frac{dm}{dt}\right] , \tag{3.4-19}$$

where

$$\tau_w = \frac{R(\Delta P_m - \rho gh)}{2L} . \tag{3.4-20}$$

Equation (3.4-19) is used to evaluate γ_w from the first and second derivatives of the $\log(\Delta P_m - \rho gh)$ versus t plot, the applied pressure across the capillary, and the dimensions of the instrument.

3.5 Pressure Flow Relations for Non-Newtonian Suspensions

Relationships between the pressure drop and the reduced average velocity for both Power and Casson fluids will be considered in this section.

The Power law equation was given in Section 3.1 as

$$f(\tau) = \left(\frac{\tau}{k}\right)^{1/n} , \tag{3.1-5}$$

where n and k are as defined in Section 3.1.

Substitution of this equation into Equation (3.2-11), following by integration between the limits 0 and τ_w, gives

$$\frac{Q}{\pi R^3} = \frac{n \, \tau_w^{1/n}}{k^{1/n}(3n + 1)} \tag{3.5-1}$$

This can also be expressed in terms of τ_w as the dependent variable as

$$\tau_w = k \left[\frac{(3n+1)}{n} \left(\frac{Q}{\pi R^3}\right)\right]^n \tag{3.5-2}$$

Equation (3.5-3) can also be expressed in terms of the pressure drop on substitution of Equation (3.2-7). The result of this operation is:

$$\Delta P = \frac{2Lk}{R} \left[\frac{(3n+1)}{n} \left(\frac{Q}{\pi R^3}\right)\right]^n \tag{3.5-3}$$

The Casson equation has also been defined in Section 3.1 as:

$$f(\tau) = \frac{1}{S^2} \left[\tau - 2\sqrt{\tau_y \tau} + \tau_y\right] \tag{3.1-6}$$

where, S and τ_y are as defined in Section 3.1. Substitution of above equation into Equation (3.2-11), followed by integration between the limits τ_y and τ_w gives after simplification:

$$\frac{Q}{\pi R^3} = \frac{\tau_w}{S^2} \left[\frac{1}{4} + \frac{1}{3}\left(\frac{\tau_y}{\tau_w}\right) - \frac{4}{7}\left(\frac{\tau_y}{\tau_w}\right)^{1/2} - \frac{1}{84}\left(\frac{\tau_y}{\tau_w}\right)^4\right] . \tag{3.5-4}$$

Inspection of Equation (3.5-4) reveals that it cannot be expressed in terms of τ_w as the dependent variable.

Consideration of the magnitudes of the terms within the brackets on the RHS of the above equation reveals that the term $\left(\frac{\tau_y}{\tau_w}\right)^4$ can be neglected for $\left(\frac{\tau_y}{\tau_w}\right) < 0.4$, (46) and thus Equation (3.5-4) can be approximated as:

$$\frac{Q}{\pi R^3} = \frac{\tau_w}{S^2} \left[\frac{1}{4} + \frac{1}{3}\left(\frac{\tau_y}{\tau_w}\right) - \frac{4}{7}\left(\frac{\tau_y}{\tau_w}\right)^{1/2}\right] , \tag{3.5-5}$$

for a wide range of τ_w ($\tau_w > 2.5\ \tau_y$). A similar approximation has been

employed for the Bingham plastic model (14).

Equation (3.5-5) can be expressed as a quadratic in $\sqrt{\tau_w}$ and solved to give an expression for τ_w in terms of Q. The algebraic manipulations result in

$$\tau_w = \frac{188}{147}\tau_y + \frac{32\ S^2\tau_y}{7}^{1/2}\sqrt{\frac{Q}{\pi R^3 S^2} - \frac{\tau_y}{147S^4} + \frac{4S^2Q}{\pi R^3}}\ . \qquad (3.5\text{-}6)$$

When $\frac{\tau_y}{147S^4}$ is small compared to $\frac{Q}{\pi R^3 S^2}$ as was the case with the experimental data in this investigation, Equation (3.5-6) can be further approximated by:

$$\tau_w = \frac{188}{147}\tau_y + \frac{32S}{7}\tau_y^{1/2}\sqrt{\frac{Q}{\pi R^3} + \frac{4S^2Q}{\pi R^3}}\ . \qquad (3.5\text{-}7)$$

The above equation can be expressed in terms of the pressure drop (ΔP), by using Equation (3.2-7); this results in

$$\Delta P = \frac{2L}{R}\left[\frac{188}{147}\tau_y + \frac{32S\ \tau_y}{7}^{1/2}\sqrt{\frac{Q}{\pi R^3} + \frac{4S^2Q}{\pi R^3}}\right]\ . \qquad (3.5\text{-}8)$$

Equations (3.5-5) and (3.5-7) can also be expressed in terms of the variable $\bar{U}$ (a variable employed by Merril and coworkers). This variable is called the average flow velocity and it is expressed in tube diameters per unit time, although it has the dimensions of sec^{-1}. This variable is defined as:

$$\bar{U} = \frac{1}{2}\frac{Q}{\pi R^3} \qquad (3.5\text{-}9)$$

Substitution of this equation into Equations (3.5-5) and (3.5-7) gives:

$$\bar{U} = \frac{\tau_w}{2S^2}\left[\frac{1}{4} + \frac{1}{3}\left(\frac{\tau_y}{\tau_w}\right) - \frac{4}{7}\left(\frac{\tau_y}{\tau_w}\right)^{1/2} - \frac{1}{84}\left(\frac{\tau_y}{\tau_w}\right)^4\right]\ , \qquad (3.5\text{-}10)$$

and

$$\tau_w = \frac{188}{147}\,\tau_y + \frac{32\sqrt{2}\,S\,\tau_y^{1/2}}{7}\sqrt{\bar{U}} + 8S^2\,\bar{U} \qquad (3.5\text{-}11)$$

respectively.

Approximation to the Casson Equation

The Casson Equation (3.1-6) can be expressed as:

$$\sqrt{\tau_w} = \sqrt{\tau_y} + S\sqrt{\gamma_w}\ , \qquad (3.5\text{-}12)$$

where $\sqrt{\tau_y}$ is the square root of the apparent yield stress and S is the Casson viscosity. These variables are sometimes denoted by k_0 and k_1 respectively.

Merril and coworkers (25), have derived an approximation to the Casson equation using the following procedure. From the Rabinowitsch equation, γ_w can be expressed in terms of $\bar{U}$ as

$$\gamma_w = 2\,\bar{U}(3 + N)\ , \qquad (3.5\text{-}13)$$

where $$N = \frac{d\ \ell n\ \bar{U}}{d\ \ell n\ \tau_w}\ .$$

Combining Equations (3.5-12) and (3.5-13) gives:

$$\tau_w^{1/2} = \tau_y^{1/2} + S[2(3 + N)]^{1/2}\,\bar{U}^{1/2} \qquad (3.5\text{-}14)$$

Merril made the assumption that N can be considered constant over limited ranges of τ_w; in this basis he has arbitrarily set N = 1 (the case of Newtonian behavior). With this assumption Equation (3.5-14) becomes:

$$\tau_w^{1/2} = \tau_y^{1/2} + 2\sqrt{2}\ S\,\bar{U}^{1/2}\ . \qquad (3.5\text{-}15)$$

When this equation is squared the following equation results:

$$\tau_w = \tau_y + 4\sqrt{2}\,|\, S\, \tau_y^{1/2}\, \sqrt{\bar{U}} + 8S^2\, \bar{U} \ . \qquad (3.5\text{-}16)$$

This is an approximation to Equation (3.5-10). A plot of $\tau_w^{1/2}$ versus $\bar{U}^{1/2}$ allows the evaluation of τ_y and S with the aid of Equation (3.5-15).

An alternate approximate Casson equation can be obtained with the aid of Equation (3.5-11). The objective of the following analysis is to find an expression relating $\sqrt{\tau_w}$ and $\sqrt{\bar{U}}$ such that when it is squared, Equation (3.5-11) results. The required expression is of the form:

$$\tau_w^{1/2} = X\, \tau_y^{1/2} + Y\, \bar{U}^{1/2} \ , \qquad (3.5\text{-}17)$$

where X and Y are the coefficients to be determined. Squaring both sides of the above equation results in:

$$\tau_w = X^2\, \tau_y + 2XY\, \tau_y^{1/2}\, \bar{U}^{1/2} + Y^2\, \bar{U} \ . \qquad (3.5\text{-}18)$$

Comparison of the coefficients of this equation with the coefficients of Equation (3.5-11) should permit the evaluation of X and Y. This comparison indicates that Equation (3.5-11) is not an exact square of an equation of the form of Equation (3.5-17). Three possibilities result from this comparison:

1. Comparison of the coefficients of $\bar{U}$ and $\tau_y^{1/2}\, \sqrt{\bar{U}}$ results in:

$$Y^2 = 8S^2 \quad \text{or} \quad Y = 2\sqrt{2}\, S$$

and

$$2XY = \frac{32\, \sqrt{2}\, S}{7} \quad \text{or} \quad X = 1.143.$$

Therefore the corresponding equation is:

$$\tau_w^{1/2} = 1.143\, \tau_y^{1/2} + 2\sqrt{2}\ S\, \bar{U}^{1/2} \ . \qquad (3.5\text{-}19)$$

2. Comparison of the coefficients of τ_y and $\bar{U}$ results in:

$$X^2 = \frac{188}{147} \quad \text{or} \quad X = 1.131$$

and $$Y^2 = 8S^2 \quad \text{or} \quad Y = 2\sqrt{2}\ S.$$

Therefore the corresponding equation is

$$\tau_w^{1/2} = 1.131\ \tau_y^{1/2} + 2\sqrt{2}\ S\ \bar{U}^{1/2} \tag{3.5-20}$$

3. Comparison of the coefficients of τ_y and $\tau_y^{1/2}\sqrt{\bar{U}}$ results in:

$$X^2 = \frac{188}{147} \quad \text{or} \quad X = 1.131$$

and $$2XY = \frac{32\sqrt{2}\ S}{7} \quad \text{or} \quad Y = 2.021\sqrt{2}\ S.$$

The corresponding equation is:

$$\tau_w^{1/2} = 1.131\ \tau_y^{1/2} + 2.021\sqrt{2}\ S\ \bar{U}^{1/2}\ . \tag{3.5-21}$$

Equations (3.5-19), (3.5-20) and (3.5-21) will be compared for a wide range of conditions in Chapter 5.

A plot of $\tau_w^{1/2}$ versus $\bar{U}^{1/2}$ can be employed for the evaluation of τ_y and S. One way to evaluate τ_y is by dividing the intercept of this plot by 1.143, and S can be evaluated by dividing the slope of this plot by $2\sqrt{2}$, in accordance with Equation (3.5-19). The other Equations (3.5-20) and (3.5-21) can be employed in a similar way for the evaluation of these parameters.

3.6 Friction Factor Relations for Non-Newtonian Suspensions

Theoretical expressions for the laminar friction factors of Power law and Casson fluids, flowing in cylindrical tubes, will be developed in this section. The generalized method of Metzner and Reed is also included.

The usual definition of the friction factor in terms of the applied pressure ΔP is given by

$$f = \frac{D\,\Delta P}{4L} \Big/ \frac{\rho U_m^2}{2}\,, \tag{3.6-1}$$

where U_m is the average velocity of the fluid in $\frac{cm}{sec}$ given by

$$U_m = Q/\pi R^2\,. \tag{3.6-2}$$

Substitution of Equations (3.6-2) and (3.2-7) into Equation (3.6-1), results in an expression for the friction factor (f) in terms of the wall shear stress and the reduced average velocity $Q/\pi R^3$.

This expression is given by

$$f = \frac{2}{\rho R^2} \frac{\tau_w}{\left(\frac{Q}{\pi R^3}\right)^2}\,. \tag{3.6-3}$$

The usual definition for the Reynolds number for a Newtonian fluid is

$$Re = \frac{D\,U_m\,\rho}{\mu}\,. \tag{3.6-4}$$

or in terms of $Q/\pi R^3$

$$Re = \frac{2\,R^2\,\rho}{\mu}\left(\frac{Q}{\pi R^3}\right)\,. \tag{3.6-5}$$

1. Power Law Fluid. An expression for the friction factor of a power law fluid in laminar flow can be obtained by multiplying both sides of Equation (3.5-3) by $[\frac{1}{4}(\frac{D}{L})]$ / $[\frac{1}{2}\,\rho\,U_m^2]$. The result can be simplified with the aid of Equation (3.6-2) and the definition for the friction factor, Equation (3.6-1)

to give

$$f = \frac{16}{R'_e} , \tag{3.6-6}$$

where R'_e is the modified Reynolds number for a power law fluid, defined as:

$$R'_e = \frac{\rho D^2 \left(\frac{Q}{\pi R^3}\right)^{2-n}}{\frac{k}{2^{n+1}} \left[\frac{6n + 2}{n}\right]^n} . \tag{3.6-7}$$

This expression is analogous to the equation for the friction factor of Newtonian fluids in laminar flow. It is also analogous to the generalized friction factor relation for laminar flow developed by Metzner and Reed (28).

2. Casson Fluid. The development given here is similar in principle to that given by Hedström (14) for Bingham plastic fluids.

An expression for the friction factor of a Casson fluid in laminar flow can be obtained by multiplying both sides of Equation (3.5-8) by $[\frac{1}{4} (\frac{D}{L})] / [\frac{1}{2} \rho U_m^2]$. The result can be simplified with the aid of Equations (3.6-1) and (3.6-2) to give

$$f = \frac{1}{Re^*} \left[\frac{376}{147} \left(\frac{He^*}{Re^*}\right) + \frac{64\sqrt{2}}{7} \left(\frac{He^*}{Re^*}\right)^{1/2} + 16\right] , \tag{3.6-8}$$

where Re^* and He^* are the modified Reynolds and Hedström numbers defined as:

$$Re^* = \frac{2 R^2 \rho}{S^2} \left(\frac{Q}{\pi R^3}\right) \tag{3.6-9}$$

and

$$He^* = \frac{\tau_y D^2 \rho}{S^4} \tag{3.6-10}$$

3. Generalized Method by Metzner and Reed. Metzner and Reed (28) have developed a universal correlation for friction factor--generalized Reynolds number data. This correlation is theoretically rigorous in the laminar flow region and is applicable to all fluids, Newtonian and non-Newtonian alike.

The Rabinowitsch equation was the starting point of the analysis given by Metzner and Reed. The Rabinowitsch equation was expressed in terms of U_m, as given below,

$$\left(-\frac{d_u}{d_r}\right)_w = \frac{3}{4}\left(\frac{8U_m}{D}\right) + \frac{1}{4}\frac{8U_m}{D} \cdot \frac{d\ \ell n\ (8U_m/D)}{d\ \ell n\ (D\ \Delta P/4L)}\ , \qquad (3.6\text{-}11)$$

where the variables here are as defined previously. In order to simplify the above equation, the derivative on the RHS of Equation (3.6-11) was denoted by the symbol $1/n'$, that is:

$$\frac{1}{n'} = \frac{d\ \ell n\ \left(\frac{8U_m}{D}\right)}{d\ \ell n\ \left(\frac{D\Delta P}{4L}\right)}\ . \qquad (3.6\text{-}12)$$

Rearrangement of Equation (3.6-11) gives:

$$-\left(\frac{d_u}{d_r}\right)_w = \frac{3n' + 1}{4n'} \cdot \frac{8U_m}{D}\ . \qquad (3.6\text{-}13)$$

where n' can be obtained from the slope of a log-log plot of $\frac{D\ \Delta P}{4L}\ (\tau_w)$ versus $\frac{8U_m}{D}$. The term $\frac{8U_m}{D}$ can be expressed in terms of the variable $Q/\pi R^3$ by using Equation (3.6-2):

$$\frac{8U_m}{D} = 4\left(\frac{Q}{\pi R^3}\right)\ . \qquad (3.6\text{-}14)$$

Experimental observations indicate that n' is very nearly a constant over

wide ranges of shear stress for a variety of non-Newtonian fluids. Under conditions of constant n', the expression given below applies. For constant n', Equation (3.6-12) can be integrated to give:

$$\frac{D\ \Delta P}{4L} = k' \left(\frac{8U_m}{D}\right)^{n'} , \tag{3.6-15}$$

where k' is a constant.

On substituting for $8U_m/D$ in Equation (3.6-15) from Equation (3.6-13) and denoting the shear stress at the wall of the tube ($D\ \Delta P/4L$) by τ_w, one obtains:

$$\tau_w = k' \left(\frac{4n'}{3n' + 1}\right)^{n'} \left(-\frac{d_u}{d_r}_w\right)^{n'} . \tag{3.6-16}$$

If n' is constant and has the value of unity, the above equation becomes:

$$\tau_w = k' \left(-\frac{d_u}{d_r}_w\right) , \tag{3.6-17}$$

which is, the familiar linear relationship between shear stress and shear rate for a Newtonian fluid. Here k' is obviously equal to μ, the Newtonian viscosity.

If n' is constant the power law model results:

$$\tau_w = k\left(-\frac{d_u}{d_r}_w\right)^{n'} , \tag{3.6-18}$$

Comparison of Equations (3.6-16) and (3.6-18) gives the following relationships (over ranges of shear stresses for which n' is constant):

$$n = n' \tag{3.6-19}$$

and

$$k = k' \left(\frac{4n'}{3n' + 1}\right)^{n'} \tag{3.6-20}$$

Equation (3.6-15) can also be expressed in terms of the friction factor, as defined by Equation (3.6-1). The resulting expression is:

$$f = \frac{16}{N_{Re}} , \tag{3.6-21}$$

where

$$N_{Re} = \frac{D^{n'} U_m^{2-n'} \rho}{8^{n'-1} k'} . \tag{3.6-22}$$

This relation indicates that all fluids, Newtonian and non-Newtonian, must follow the f versus N_{Re} relationship in the laminar-flow region when one uses the generalized Reynolds number defined by Equation (3.6-22).

According to Metzner and Reed, the above development is completely rigorous and may in fact, be used to check the accuracy of experimental data. If perfect coincidence with the $f = 16/N_{Re}$ line is not obtained in the laminar flow region then either the data or calculations are in error.

CHAPTER 4

EXPERIMENTAL

The experimental studies of this investigation consisted of the measurement of the pressure drop across a long length of coiled capillary tube and the corresponding average flow velocity through a flowmeter tube, for the flow of a time independent non-Newtonian suspension. From this information the volumetric rate through the capillary, the wall shear stress and the wall shear rate can be evaluated.

The apparatus, shown schematically in Figure 5, consists primarily of a coiled polyethylene capillary connected between two flowmeters graduate tubes. Application of a pressure to the LHS results in flow through the capillary to the RHS. The average velocity of flow in the flowmeter can be evaluated from the rate of travel of the fluid in the RH tube. The apparatus employed was a low-shear capillary viscometer, basically similar in construction to the apparatus recently described by Benis (2).

The components of the experimental apparatus, the methods of calibration, the operating procedures, the limitations and the range of variables will be considered in this chapter.

4.1 Apparatus

The experimental apparatus is shown schematically in Figure 5. The components of the apparatus and their functions are the following:

Capillary tubing: An 800 cm length of "Intramedic" polyethylene tubing (size P.E. 190 and I.D. 0.047") was employed as the viscometer capillary.

Plexiglass spool: The capillary tubing was coiled around this spool which was 11.5 cm in diameter. The design was such that it could be readily filled

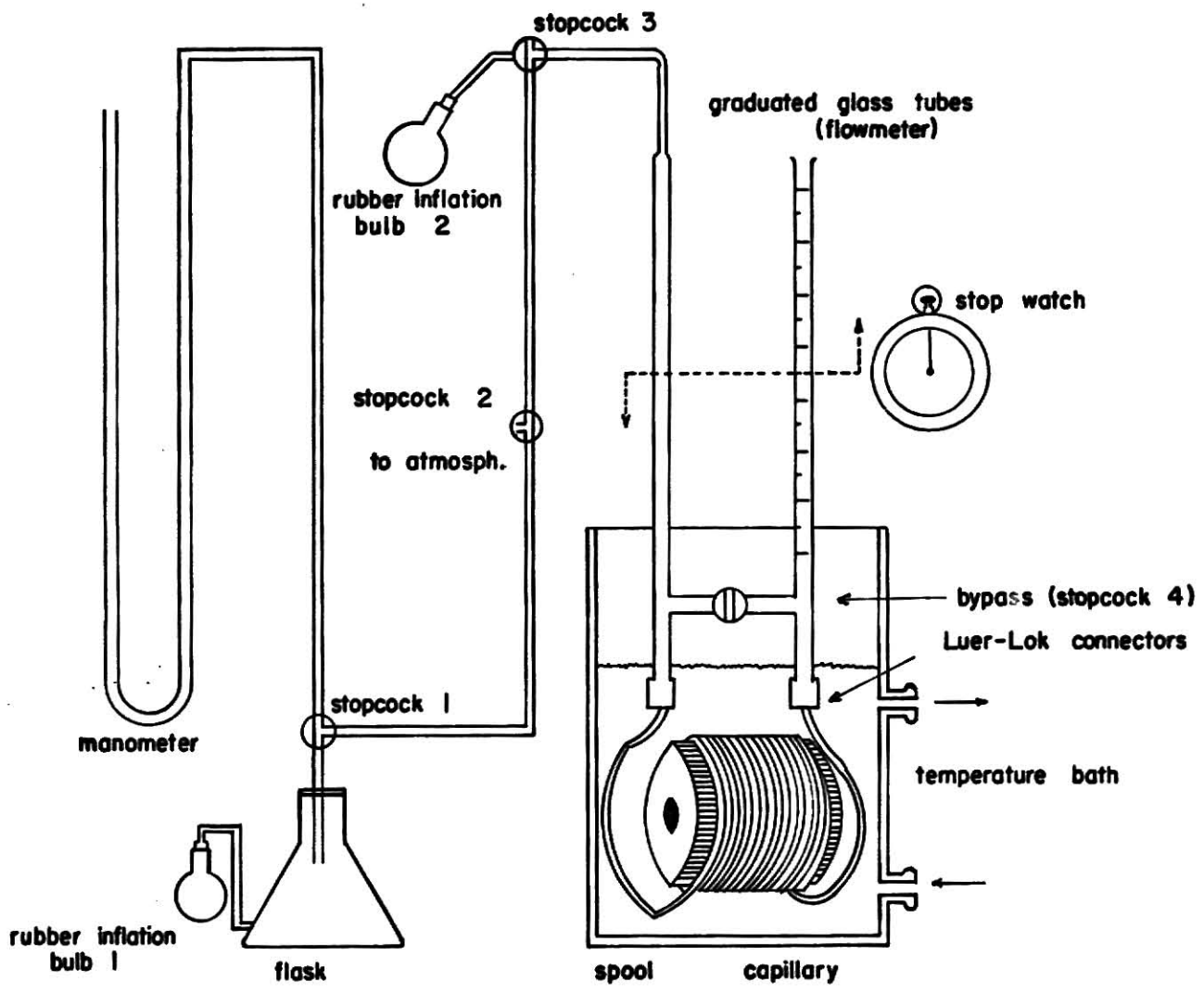

Fig. 5. Sketch of the apparatus.

with water for rapid immersion in the constant temperature bath.

Luer-Lok adapters: These adapters [size B(7551)] were used to connect the capillary tube to the flowmeters.

Flowmeters: These were used to obtain average velocity data. Two flowmeter tubes of the same diameter were connected to the capillary as indicated in Figure 5. Three types of flowmeters were used. The relevant geometric data are presented in Table 1.

TABLE 1

PHYSICAL DIMENSIONS OF THE FLOWMETERS

Type of Flowmeters	Total Volume (ml)	Inside Diameter (cm)	Divisions
Graduate	25	0.940	25 ml x $\frac{1}{10}$ th
Graduate	10	0.798	10 ml x $\frac{1}{20}$ th
Capillary	3	0.278	---

The 25 ml graduate flowmeters were used for suspensions of high concentration, in the region of shear rate (50 - 500) sec^{-1}. The 10 ml graduate flowmeters were used, with suspensions of low concentration, in the shear rate region of (30 - 1500) sec^{-1}. Both 25 and 10 ml graduate flowmeters had a side arm which was used for connecting a bypass between them.

The capillary flowmeters were "true bore" capillary glass tubes and they were used for low solid concentration in shear rate region of (4 - 150) sec^{-1}. Two small "T" tubes were joined to the "true bore" capillaries, in order to bypass the polyethylene capillary.

Bypass: A piece of tubing with a two way stopcock in the middle was connecting between the RHS and LHS flowmeters to provide a bypass. This was employed primarily to facilitate mixing of the suspension in between experimental runs.

Pressure supply: A 3000 cc chamber was employed as an air reservoir. Air was introduced using a rubber inflation bulb. (See Figure 5, rubber inflation bulb 1.) The air pressure was read on a "U" tube manometer connected to the air chamber as indicated in Figure 5. The pressure was applied across the capillary, by connecting the air reservoir to the LHS flowmeter, as indicated in the same figure.

Stopcocks: The pressure line connecting the air chamber and the LHS flowmeter contained three stopcocks. (See Figure 5.) The first one, a three way stopcock, was used to connect the pressure chamber to the manometer. This stopcock was used in place of a "T" connector.

Stopcock No. 2, was a three way stopcock which permitted venting of the reservoir and the viscometer as well as application of a pressure to the capillary.

Stopcock No. 3, also a three way stopcock was used to connect the viscometer to an additional rubber inflation bulb. This bulb (see Figure 5, rubber inflation bulb 2) was employed for the agitation of the suspensions in between runs. This minimized settling of silica suspensions without changes in the air pressure in the air chamber. This feature represents an improvement over the Benis viscometer.

Constant temperature bath: The viscometer was thermostated at 25°C ± 0.2°C in a constant temperature bath. Only the coiled capillary was immersed in the bath, as suggested by Benis (2).

Connecting tubing: Rubber tubes, 1/4" ID, were used to connect the manometer, air chamber and the viscometer together.

Cathetometer: A Griffin intermediate cathetometer with an accuracy of ± 0.01 cm, was used for measuring the rate of travel of the meniscus in the flowmeter tube when working at low rates, as well as for reading the pressure difference from the manometer.

Stopwatch: A Meylan stopwatch, Model 410, was used for timing the rate of travel of the meniscus up the flowmeter. This stopwatch can be read to 0.1 second.

pH Meter: A Fisher Accumet pH meter, model 210 was used for making measurements in the pH of the suspensions.

4.2 Materials

The suspensions were prepared by mixing silica particles with demineralized water. The silica was obtained from Illinois Minerals Company. The silica employed (grades IMSIL A-10 and IMSIL A-15) had an average specific gravity of 2.65. Tables 9, 10 and 11 in Appendix A show the most important characteristics, chemical analysis and physical properties.

The demineralized water was prepared by passing tap water through a Barnstead demineralizer containing a mixed resin bed cartridge. The pH of the demineralized water was 6.4.

The silica particles were spherical with varying diameters from 5 to 40 microns, dependent on the grade. Table 9 shows particle size for two different grades of silica.

The pH of the suspensions was fixed at 7.0 for all experiments because it has been shown that the flow properties of the silica suspensions are dependent on this parameter (30).

The silica suspensions were prepared by placing a given weight of silica in a beaker and adding demineralized water to obtain the desired solid concentration.

The concentration was expressed in terms of volume fraction of solids, ϕ, defined as volume of solute in ml over total volume of solution. For low solid concentration, 54 gr of silica were mixed with 380 ml of water. Since the average specific gravity of silica was 2.65, and assuming no change in volume of mixing the corresponding solid concentration was $\phi = 0.05$. For high solid concentration, 212 gr of silica were mixed with 320 ml of water. The corresponding solid concentration was $\phi = 0.20$. The mixture was first stirred thoroughly with a glass rod and then with a magnetic stirrer in a closed container for more than one hour.

After mixing, a sample was taken for a pH measurement. The remaining solution was continuously stirred. The pH of the suspensions ranged between 7.2 and 7.4. It was adjusted to a pH of 7.0 by adding 1N HCl dropwise.

Settling of silica suspensions was present after approximately 200 seconds without stirring, as indicated by comparisons with flow data.

4.3 Calibration Procedure

The methods of calibration of the flowmeters and the capillary tubes are presented in this section.

Calibration of capillary flowmeters. The radius of the "true bore" capillary flowmeter tube was determined by filling with mercury and weighing the thread of mercury contained in the capillary. The capillary radius was calculated after measurement of the capillary length with the aid of the formula for the volume of a cylinder and the density of mercury at the temperature of the filling. Three different lengths of capillary were used and the average

radius was calculated.

Calibration of the graduate flowmeters. The purpose of calibrating the capillary tube is to precisely determine its inside diameter. The cross sectional area of the graduate flowmeters was calculated after measurement of the length between two graduate divisions by using the cathetometer. The readings were taken between 0 and 25 marks for the 25 ml flow meters and between 0 and 10 marks for the 10 ml flowmeters. Several readings were taken and the results were averaged.

Calibration of the capillary tube. An 800 cm length of capillary tube was coiled onto the spool and connected to the flowmeters by means of Luer-Lok connectors. Distilled water was used as the calibrating fluid. The calibration was conducted with both the capillary and graduated flowmeter tubes.

The apparatus was filled with approximately 20 ml of water (when graduate flowmeters were used) and approximately 10 ml (when capillary flowmeters were used). With the bypass closed, water was introduced by means of a syringe through the RHS of the capillary with the LHS and being connected to the flowmeter. After the liquid had been injected, the free end of the capillary was connected to the RHS flowmeter. The meniscus was permitted to travel a few centimeters in the RHS flowmeter before opening the bypass, thus minimizing the trapping of bubbles in the filling process.

The apparatus was then examined for trapped air bubbles which, if necessary, were eliminated before proceeding. Stopcock 3 and the bypass were closed and care was taken to insure that the liquid levels in the two flowmeters were equal. The viscometer was then placed in the constant temperature bath. A selected pressure was then applied to the air reservoir, this pressure was read on the manometer by means of the cathetometer.

Stopcock 2 was then opened allowing the fluid to flow through the capillary. The stopwatch was started at the instant stopcock 2 was opened. The average velocity of the fluid in the RHS flowmeter was measured by timing the meniscus at several points as it flowed up the flowmeter. When the flow-time was of the order of 200 sec, stopcock 2 was closed and the bypass was opened allowing the liquid levels in both flowmeters to be restored to the equilibrium level. This procedure was repeated at the same pressure, to obtain another set of flowtimes. The average of these flowtimes was employed in the calculations.

A wide range of pressures was employed. These ranged from 28 cm Hg to 20 cm of H_2O when working with graduate flowmeters and from 10 cm of Hg to 12 cm of H_2O when the capillary flowmeters were used.

The cathetometer was used to take readings in the graduate flowmeter at low pressures, and for all readings in the capillary flowmeters.

At low pressures (water manometer) there was a perceptible small change in the pressure after stopcock 2 was opened to the system. Therefore a new reading of the pressure was necessary to make the appropriate correction in the applied pressure.

At the end of each run, another reading of the pressure was taken because it did not stay sufficiently constant in some of the experiments. Variations of pressure with time can be calculated to make the corrections to the pressure at every point where the meniscus was timed.

4.4 Procedure with Silica Suspensions

The procedure for filling the viscometer and for taking flow data for silica suspensions was identical to the procedure followed for the calibration of the capillary tube using distilled water, as was pointed out in

Section 4.3.

However, one additional operation was used here to minimize settling. In between runs the suspension was mixed with the aid of the pressure applied with the extra rubber inflation bulb. This operation was repeated over time intervals no longer than four minutes.

Two sets of data were obtained at the same pressure and the average of flowtimes was employed in the calculations.

Cleaning of the viscometer. The following steps were carried out for cleaning the viscometer.

1. The Luer-Lok connectors were disconnected, allowing the liquid inside the flowmeter to drain.

2. The flowmeters, bypass and Luer-Lok connectors were flushed with distilled water.

3. Distilled water was forced through the capillary tube by means of a syringe. The silica suspension was displaced completely and the capillary was flushed several times with distilled water.

Range of variables. Table 2 shows the range of variables encountered in the experimental study.

Limitations. The maximum applied pressure that can be employed with this instrument with fluids of low consistency is of the order of 30 cm Hg. Applied pressures of this magnitude and higher results in significant inertial losses which are not attributable to the capillary alone. This was indicated by the calibration procedure noting that at pressures higher than 30 cm of Hg, an additional resistance to the flow was presented. This was mainly due to inertial pressure losses in the connectors, resulting from the high flow and the abrupt expansions and contractions in this region.

TABLE 2

RANGE OF VARIABLES

ϕ	Flowmeter type	Range of ΔP	Meniscus differences in between readings (cm)	τ_w $(\frac{dyne}{cm^2})$	$Q(\frac{ml}{sec})$	γ_w (sec^{-1})
0.05	Capillary Flowmeters	45-20 cm H_2O	2.0 - 0.5	1.42 - 0.14	0.01 - 0.001	142.0 - 10.4
0.05	10 ml	25 cm Hg - 20 cm H_2O	2.0 - 0.2	10.7 - 0.6	0.122 - 0.006	1092.0 - 60.0
0.20	25 ml	23.13 cm Hg - 65.18 cm H_2O	1.44 - 0.15	10.52 - 2.14	0.003 - 0.003	435.0 - 14.7

The maximum flow time that can be employed with this instrument is of the order of 200 sec. It was found that significant settling of the silica particles took place for flow times which exceeded this value. This effect gives a false indication of non-Newtonian behavior. This situation was observed for $\phi = 0.05$. The criteria for flow time less than 200 sec was also applied to silica concentrations of $\phi = 0.20$.

CHAPTER 5

RESULTS AND DATA ANALYSIS

The results of the calibration of the flowmeters and capillary tubes, and the analysis of silica suspension data, are presented in this chapter. From these data, the flow curves are constructed and the various approximate equations and expressions for friction factors developed in Chapter 3 are examined.

5.1 Calibration and Data Analysis

Calibration of flowmeter tubes. The procedure for the calibration of the three types of flowmeters used in this investigation was outlined in Section 4.3. The results of these calibrations are presented in Table 3.

TABLE 3

CALIBRATION OF FLOWMETERS

Flowmeter Type	Cross Sectional Area (cm^2) (A)	Radius (cm) (R_F)
Capillary	0.0607	0.139
10- ml	0.500	0.399
25- ml	0.694	0.470

General procedure for the analysis of data. The data analysis outlined below applies to both the calibration of the capillary tube and the analysis of silica suspension flow data.

Measurements of h^* (the height of the fluid in the RHS flowmeter relative to its equilibrium position) versus time were made at several applied

pressures ΔP_m. The details of this procedure have been presented in Sections 4.3 and 4.4.

The pressure drop across the capillary, $\Delta\rho_m - \rho gh$, was then calculated at each t (recall $h = 2h^*$). In addition the wall shear stress values were calculated from the relation:

$$\tau_w = \frac{R(\Delta P_m - \rho gh)}{2L} \tag{3.4-20}$$

Data were plotted in the form of log $(\Delta P_m - \rho gh)$ versus t, and the slope (m) was evaluated. For some data, the plots were linear (particularly the calibration data) and for other data the plots were non-linear. In the case of non-linear plots the slope was evaluated at each t.

Calibration of the capillary tube. This calibration was carried out with distilled water as described in Section 4.3. Data (h^* versus t) were obtained with both the capillary and graduate flowmeters on a wide range of applied pressure (11 cm $H_2O < \Delta P_m <$ 28 cm Hg). The log $(\Delta P_m - \rho gh)$ versus t plots resulted in straight lines, as expected. The capillary radius was calculated from the slope of the plot for each applied pressure with the aid of Equations (3.4-14) and (3.4-15). The following relation was used to find the capillary radius:

$$R_c^4 = \frac{9.212\ L\ R_f^2\ \mu\ m}{g\ \rho} \tag{5.1-1}$$

where μ and ρ are the reported values of the viscosity and the density of water at 25°C. The average (arithmetic) experimental radius was then calculated for the data with each flowmeter. Two capillaries (both 800 cm long) obtained from the same spool were employed in this study. The results of the calibration are presented in Table 4. Good agreement in the capillary radius

was obtained over the wide range of pressures employed as indicated in Table 4.

TABLE 4

CALIBRATION OF THE CAPILLARY TUBES

Flowmeter Type	Tube 1 R_c (Average) (cm)	Tube 2 R_c (Average) (cm)
Graduate	0.0523 (10 ml) ± 0.0002	0.0550 (25 ml) ± 0.0002
Capillary	0.0526 ± 0.0002	

A small difference in the capillary radius (Tube 1) was obtained with both flowmeters. However this difference was small enough and can be attributable to experimental error. The capillary radius obtained with the graduate flowmeters was used in the calculations because results obtained at high pressure are less subject to experimental errors.

A small difference was obtained in the calibration of tubes 1 and 2, in spite of being obtained from the same spool. However this variation is expected because the capillary tube is not a "true bore."

Figures 6 and 7 illustrate typical results of $\log(\Delta P_m - \rho gh)$ versus t plots for distilled water at 25°C. The results presented here are for both types of flowmeters at high and low pressure. Excellent straight lines were obtained as can be seen in Figures 6 and 7. For pressures of 30 cm of Hg and higher, plots of $\log(\Delta P_m - \rho gh)$ versus t were not straight lines. This was a result of additional contributions to the resistance from the Luer-Lok connectors under conditions of fast flow (inertial losses). As a consequence applied pressures above 30 cm of Hg were not employed in this study.

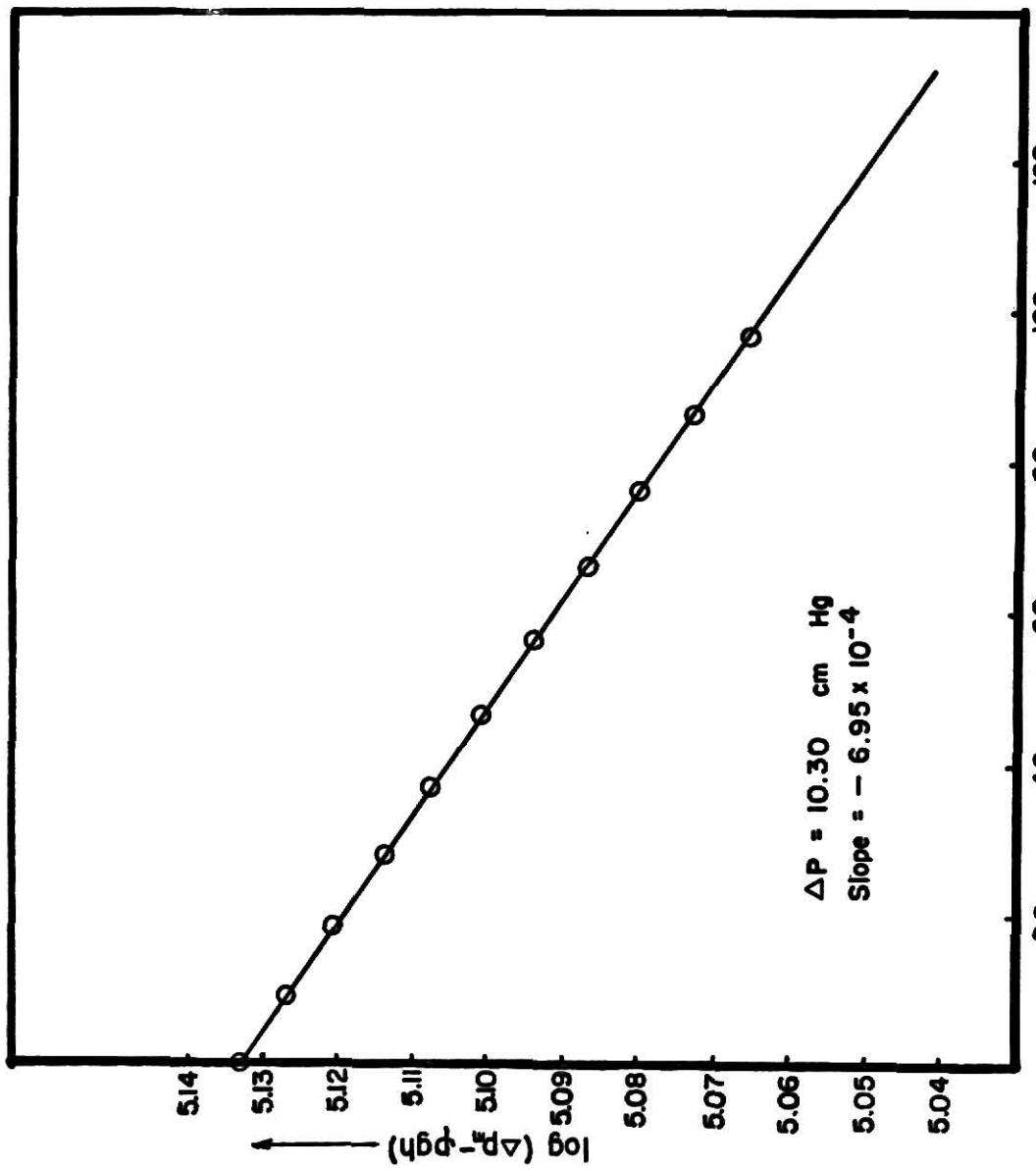

Fig. 6 . Plot of $\log(\Delta p_m - \rho gh)$ vs. time for distilled water using the 10 ml. flowmeter.

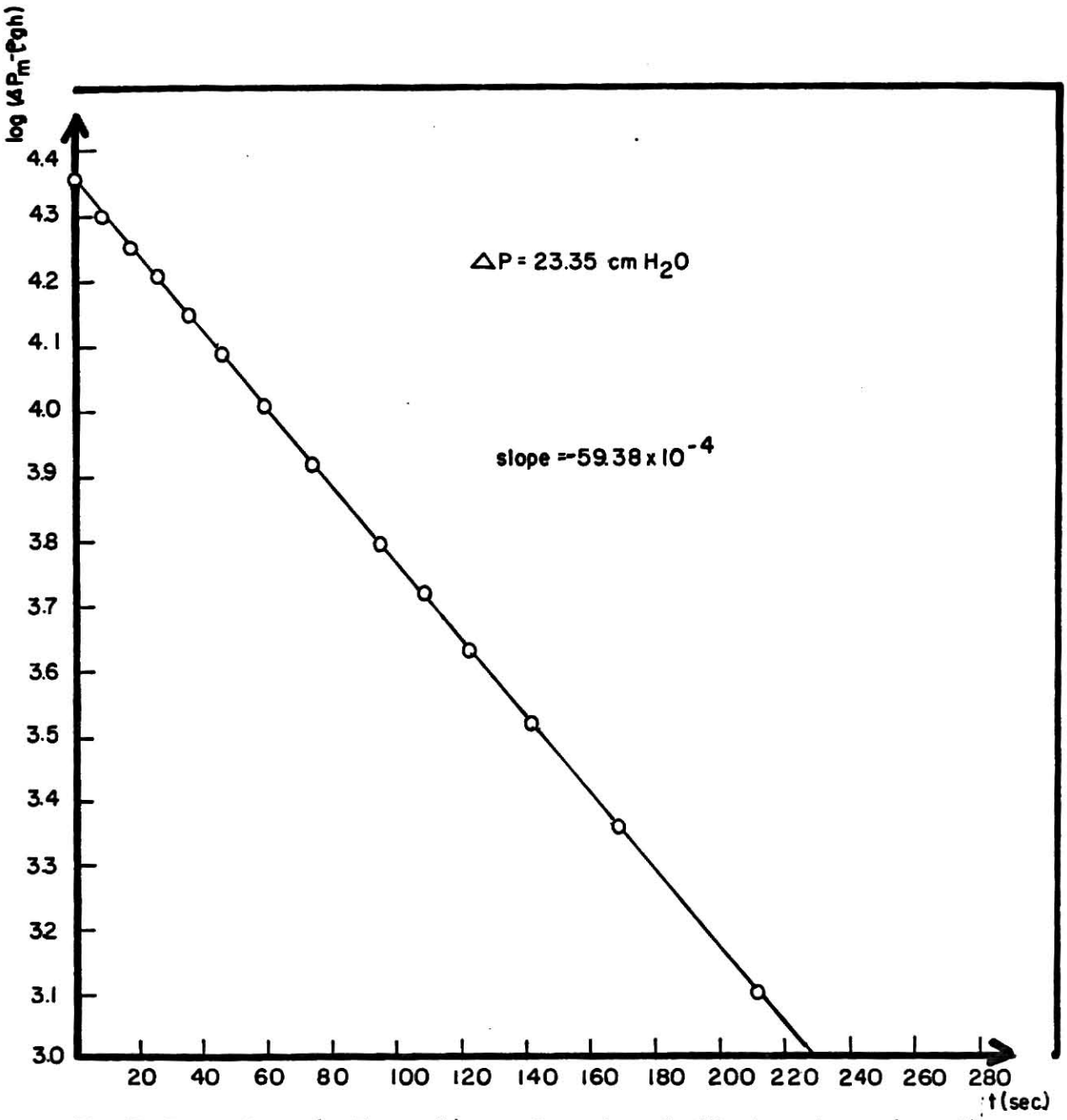

Fig. 7. Plot of log ($\Delta P_m - \rho gh$) vs time for distilled water, using the capillary Flowmeters.

Silica suspension data. Data (h^* versus t) were obtained with silica suspensions (ϕ = .05 and ϕ = .2) as described in Section 3.4, and plotted in the form of $\log(\Delta P_m - \rho gh)$ vs t for each applied pressure. When these plots resulted in straight lines, the shear rate values (γ_w) can be calculated from:

$$\gamma_w = \frac{\tau_w m}{B \rho} . \qquad (5.1\text{-}2)$$

The above equation is a simplification of Equation (3.4-19) for the case of dm/dt = 0. Linear data resulted for Newtonian flow and also for non-Newtonian flow over a limited range of shear stress.

When the $\log(\Delta P_m - \rho gh)$ versus t plots were not straight lines the slope m was determined at every t. These plots did not have much curvature and therefore slopes could not be obtained directly with accuracy. To obviate this difficulty, the following treatment of data given by Maron and coworkers (22) was employed. First, a known straight line lying close to the $\log(\Delta P_m - \rho gh)$ vs t plot is constructed. Next differences (δ) are calculated between the $\log(\Delta P_m - \rho gh)$ curve and the constructed line at selected values of t.

If the equation of the constructed straight line is designated by:

$$\log(H) = a + bt \qquad (5.1\text{-}3)$$

where a and b are constants that can be readily evaluated from the constructed line, then

$$\begin{aligned} \delta &= \log(\Delta P_m - \rho gh) - \log(H) \\ &= \log(\Delta P_m - \rho gh) - a - bt \end{aligned} \qquad (5.1\text{-}4)$$

Differentiation of the above equation with respect to t gives:

$$\frac{d\delta}{dt} = \frac{d \log(\Delta P_m - \rho gh)}{dt} - b \ , \qquad (5.1\text{-}5)$$

and hence

$$\frac{d \log (\Delta P_m - \rho gh)}{dt} = m = \frac{d\delta}{dt} + b \ . \qquad (5.1\text{-}6)$$

On plotting δ vs t and differentiating the curve at various points, $\frac{d\delta}{dt}$ is obtained; and this quantity when added to b yields m. A plot of $\frac{d\delta}{dt}$ versus t can be employed to evaluate the second derivative (dm/dt).

Following this method values of δ were determined at the experimental values of t for each plot. A standard least squares computer program, presented in Appendix B, was used to fit the best polynomial for the obtained δ vs t values. The data were also examined by graphical analysis. Values of m and dm/dt were calculated at every t, and the wall shear rates (γ_w) were then evaluated by using Equation (3.4-19).

$$\gamma_w = \frac{\tau_w \, m}{B \, \rho} \left[1 + \frac{1}{9.212 \ m^2} \frac{dm}{dt}\right] \qquad (3.4\text{-}19)$$

Figures 8 and 9 illustrate typical results of $\log(\Delta P_m - \rho gh)$ vs t plots for solid concentrations of $\phi = 0.05$ and $\phi = 0.20$ respectively. Figure 8 was obtained for $\Delta P_m = 44.11$ cm H_2O, using the capillary flowmeters. Deviation from the Newtonian behavior is seen clearly from this plot.

Two different lines corresponding to $\Delta P = 23.13$ cm Hg and $\Delta P = 20.17$ cm Hg respectively, are presented in Figure 9. They were obtained for high solid concentration and using the 25 ml flowmeters. Note that although both plots are linear, the slopes at each applied pressure are different, thus indicating non-Newtonian behavior.

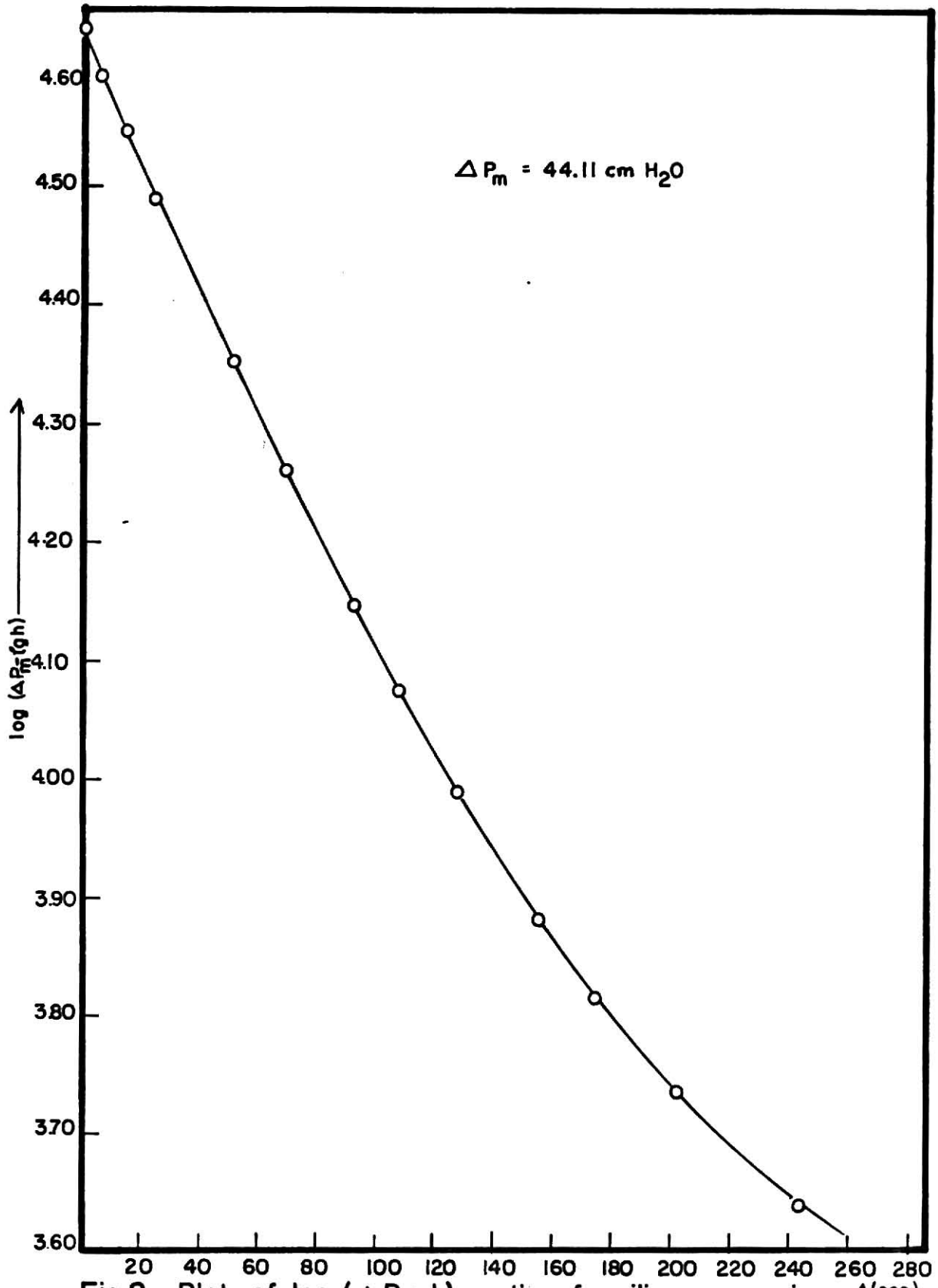

Fig. 8 Plot of log ($\Delta P_m - \rho gh$) vs time for silica suspension concentration of $\phi = 0.05$, using the capillary flowmeters.

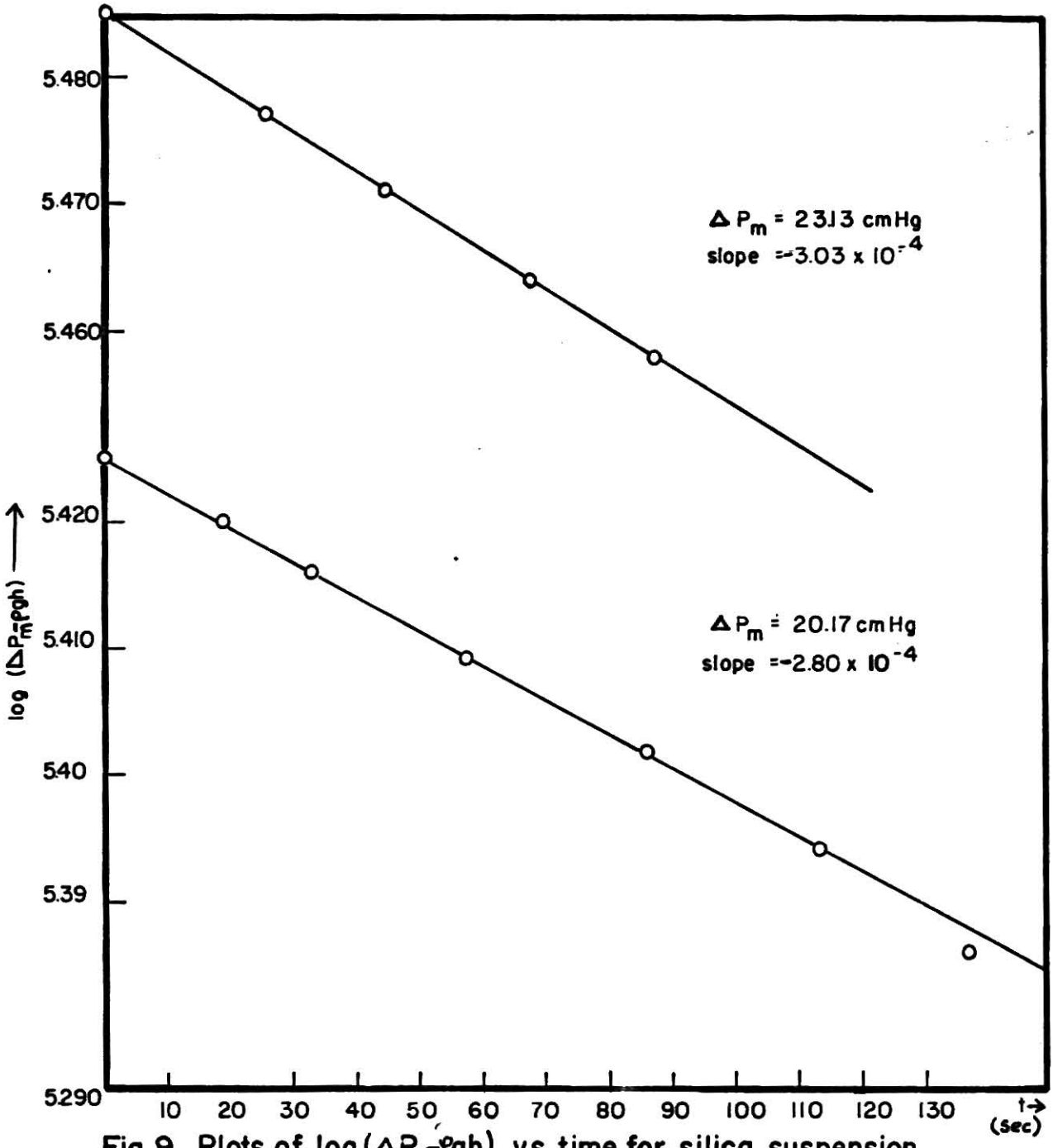

Fig. 9. Plots of log $(\Delta P_m - \rho gh)$ vs time for silica suspension concentration of $\phi = 0.20$, using the 25 ml Flowmeters.

For low solid concentrations and high applied pressures it was observed that the $\log(\Delta P_m - \rho gh)$ versus t plots were straight lines having the same slope. This indicates Newtonian behavior.

For low solid concentration and low applied pressures these plots showed curvature thus indicating non-Newtonian behavior. It should also be noted that a wide range of τ_w was covered for every applied pressure in this region, in comparison with the case of high ΔP_m. For high solid concentrations the range of τ_w covered was small. $\text{Log}(\Delta P_m - \rho gh)$ vs t were straight lines but their slopes decreased in absolute value as the applied pressure decreased. For this case, τ_w and the corresponding γ_w were calculated for $t = 0$. This procedure was employed since τ_w may change slightly with h^* whereas the slope does not change perceptibly.

A maximum flow time of 200 sec was not exceeded in any of the reported data. Observations indicated that significant settling of silica particles took place for higher values of flow times. This behavior is indicated by comparison of overlapping data in which the 200 sec flow time is exceeded.

5.2 Flow Curves and Rheological Behavior of Silica Suspensions

The experimental values of τ_w and γ_w were examined for fit to both the Power law and Casson models. In addition the Casson model approximations developed in Section 3.5 were examined.

Power law model analysis. The experimental values of τ_w and γ_w were plotted in the form of $\log(\tau_w)$ versus $\log(\gamma_w)$. For a power law fluid a straight line should result. Lines were obtained for both values of solids concentration. The results indicate regions of power law behavior.

In Figure 10 the results are shown for a solids concentration of $\phi = 0.05$. Two well defined regions can be seen. A Newtonian region with

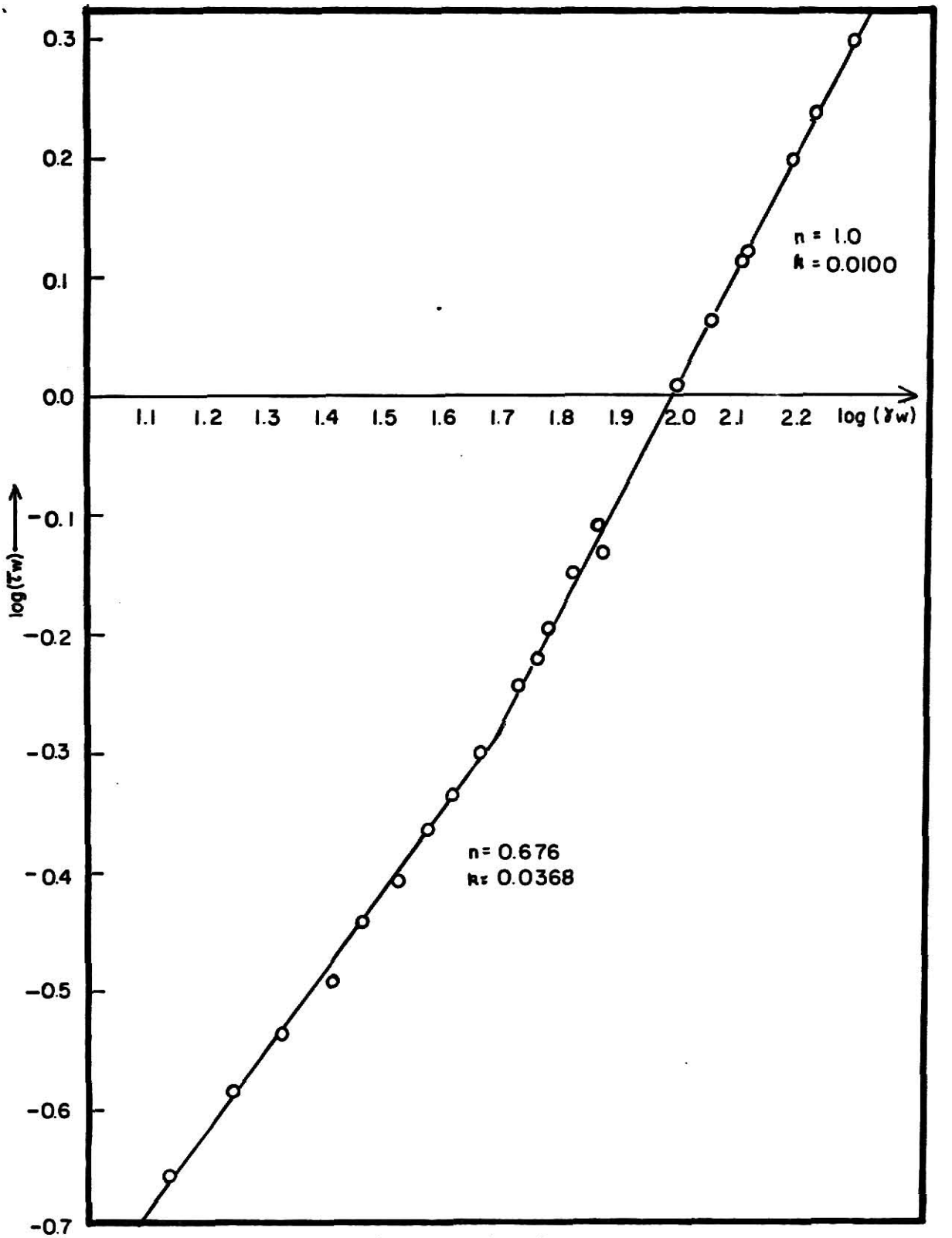

Fig. 10. Plot of log (τ w) vs log (γ w) for silica suspension concentration of ϕ=0.05 using both, Ten ml graduate and capillary Flowmeters.

Power law parameters of n = 1.0 and k = 0.01 [gm cm^{-1} sec^{-n}], and a non-Newtonian region with n = 0.676 and k = 0.0368 [gm cm^{-1} sec^{-n}]. With ϕ = 0.20 only the non-Newtonian region was observed with Power law parameters of n = 0.712 and k = 0.1389 [gm cm^{-1} sec^{-n}]. The experimental data appear to be reasonably well described by the Power law model in the non-Newtonian region over the range of shear rates which were examined.

Evaluation of $Q/\pi R_c^3$ and $\bar{U}$. The reduced average velocity $Q/\pi R_c^3$ was calculated from the following equation:

$$\frac{Q}{\pi R_c^3} = \frac{R_F^2}{R_c^3}\frac{dh^*}{dt} , \qquad (5.2\text{-}1)$$

where R_F and R_c are the flowmeter and the capillary radii respectively. The above equation is obtained by dividing both sides of Equation (3.4-9) by πR_c^3.

Plots of h^* versus t were prepared for each set of data. The slope $(\frac{dh^*}{dt})$ was evaluated from the plot when it was linear. If a curve was obtained, a least squares computer program presented in Appendix B was used to find the best polynomial fit between h^* and t. Derivatives $\frac{dh^*}{dt}$ were then calculated at the experimental values of t.

Values of $\bar{U}$ were calculated by multiplying $Q/\pi R_c^3$ by 0.5 in accordance with Equation (3.5-9). These additional values were employed in the data analyses to follow in the remaining sections of this chapter.

Casson model analysis. The experimental values of τ_w and γ_w were plotted in the form of $\sqrt{\tau_w}$ versus $\sqrt{\gamma_w}$ for each solids concentration. The lower curve in Figure 11 shows the results for a solids concentration of ϕ = 0.05. These data were obtained with both, 10 ml and capillary flowmeters. As can be seen, two well defined regions exist. At the higher shear rates the

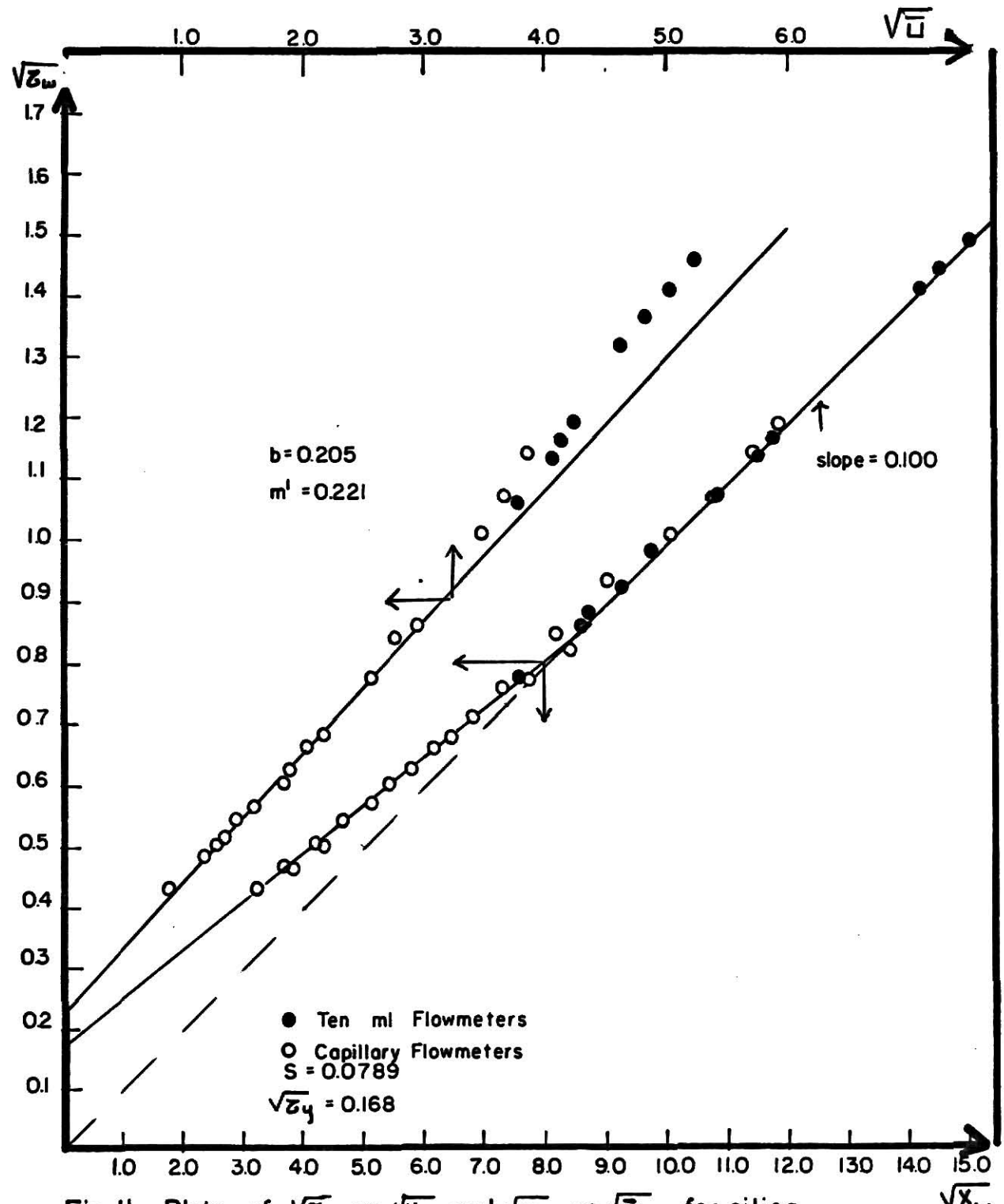

Fig. 11. Plots of $\sqrt{\tau_w}$ vs $\sqrt{\gamma_w}$ and $\sqrt{\tau_w}$ vs $\sqrt{\bar{u}}$, for silica suspension concentration of $\phi = 0.05$.

experimental points fall on a straight line passing through the origin indicating Newtonian behavior. The square of the slope of this line is equal to 0.01; this is the Newtonian viscosity and is identical to that obtained by the Power law analysis. The slope was calculated by fitting a polynomial of the form y = bx, using the least squares computer program presented in Appendix B.

For $\sqrt{\tau_w} < 0.8$ and $\sqrt{\gamma_w} < 8.0$, the experimental points fall on a different straight line having a slope S = 0.0789 and an intercept of $\sqrt{\tau_y} = 0.168$. These parameters were also calculated with the aid of the least squares computer program. Hence, non-Newtonian behavior is present in this region, and the experimental data appear to be well described by the Casson model over the range examined.

For the case of $\phi = 0.20$ only the non-Newtonian region was observed and it was well described by the Casson model as it can be seen in the lower curve of Figure 12. The values of the parameters $\sqrt{\tau_y}$ and s were also calculated by computer fit. The results were $\sqrt{\tau_y} = 0.662$ and S = 0.126.

Plots of $\sqrt{\tau_w}$ versus $\sqrt{\bar{U}}$ were obtained for both solids concentration. For $\phi = 0.05$ the experimental points in the non-Newtonian region fall on a straight line having a slope m' = 0.221 and an intercept of b = 0.205. The corresponding plot is shown as the upper curve of Figure 11. For $\phi = 0.20$ a straight line was also obtained as can be seen from the upper curve of Figure 12. This line had a slope m' = 0.365 and an intercept of b = 0.753. These parameters were obtained in both cases by computer fit.

According to Section 3.5, values of $\sqrt{\tau_y}$ and S can be obtained from the $\sqrt{\tau_w}$ versus $\sqrt{\bar{U}}$ plot, with the aid of Equations (3.5-19), (3.5-20) and (3.5-21). Values of the $\sqrt{\tau_y}$ and S were obtained by dividing the intercept b, and the

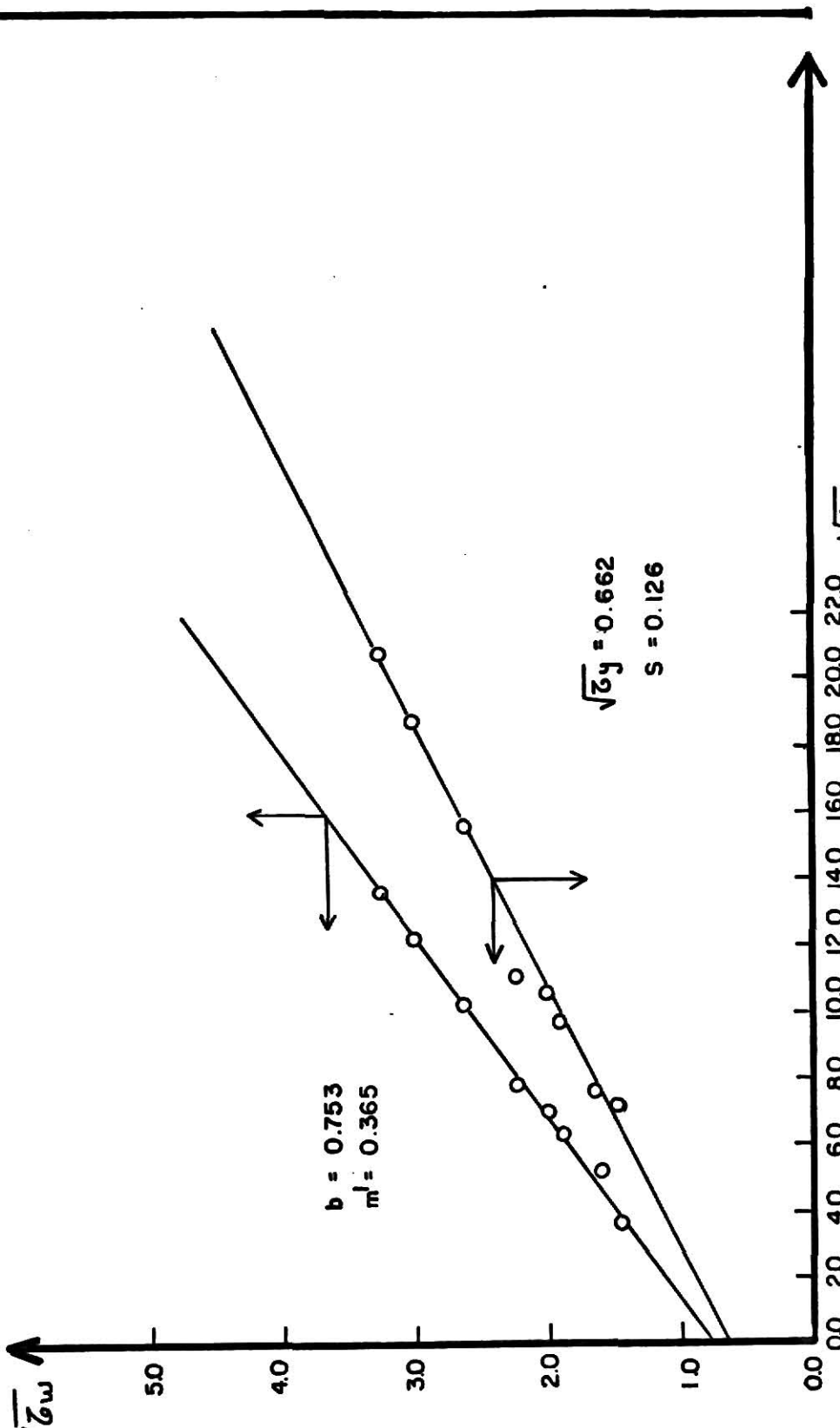

Fig. 12 Plots of $\sqrt{\tau_w}$ vs $\sqrt{\gamma_w}$ and $\sqrt{\tau_w}$ vs $\sqrt{\mu}$, for silica suspension concentration of ϕ=0.20.

slope m' of $\sqrt{\tau_w}$ versus $\sqrt{\bar{U}}$ plots by the corresponding coefficients in each of the three equations.

Calculated values of τ_y and s from $\sqrt{\tau_w}$ versus $\sqrt{\gamma_w}$ and from $\sqrt{\tau_w}$ versus $\sqrt{\bar{U}}$ plots for both solids concentrations are compared in Table 5 for each of the three forms and Equation (3.5-12).

TABLE 5

COMPARISONS OF τ_y AND S VALUES

Eq. No.	Equation	τ_y		S	
		ϕ=0.05	ϕ=0.20	ϕ=0.05	ϕ=0.20
(3.5-12)	$\sqrt{\tau_w} = \sqrt{\tau_y} + S\sqrt{\gamma_w}$	0.0280	0.438	0.0789	0.126
(3.5-19)	$\sqrt{\tau_w} = 1.143\ \sqrt{\tau_y} + 2\sqrt{2}\,\lvert\ S\sqrt{\bar{U}}$	0.0322	0.434	0.0781	0.129
(3.5-20)	$\sqrt{\tau_w} = 1.131\ \sqrt{\tau_y} + 2\sqrt{2}\ S\sqrt{\bar{U}}$	0.0329	0.443	0.0781	0.129
(3.5-21)	$\sqrt{\tau_w} = 1.131\ \sqrt{\tau_y} + 2.021\ \sqrt{2}\ S\sqrt{\bar{U}}$	0.0329	0.443	0.0773	0.128

As can be seen from the above table fairly good agreement in τ_y and s was obtained between the three approximate forms of Casson fluid and Equation (3.5-12). It may be of interest to mention here that Merril and coworkers (25) working with blood flow have obtained identical values for τ_y from $\sqrt{\tau_w}$ versus $\sqrt{\bar{U}}$ and $\sqrt{\tau_w}$ versus $\sqrt{\gamma_w}$ plots. Their approximate equation relating $\sqrt{\tau_w}$ with $\sqrt{\bar{U}}$ is given by Equation (3.5-15).

The experimental data were also plotted in the form of τ_w versus $Q/\pi R_3$. These data are presented in Figures 13 and 14 for low and high solids concentrations respectively.

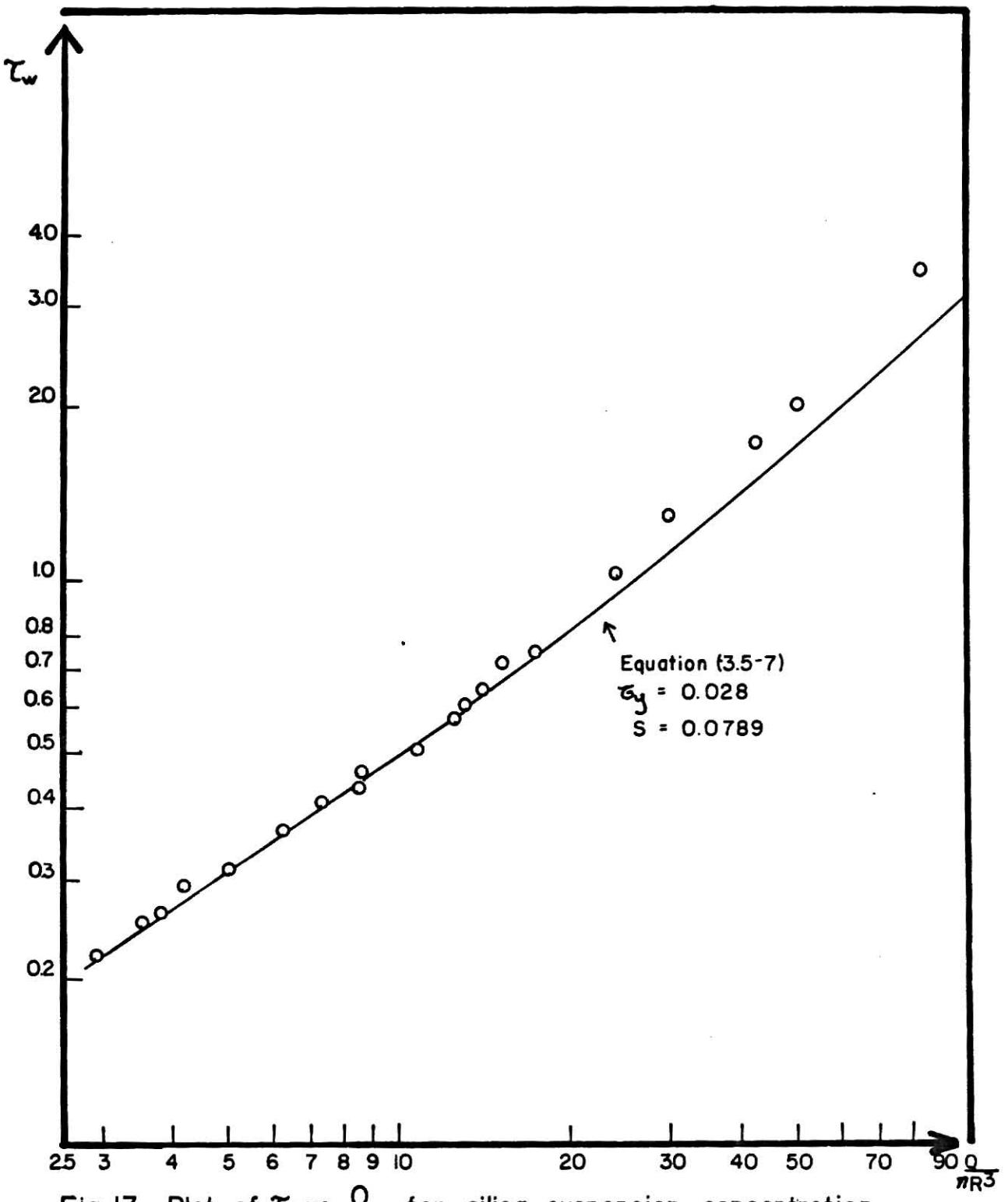

Fig. 13. Plot of τ_w vs $\frac{Q}{\pi R^3}$ for silica suspension concentration of ϕ= 0.05, using both, capillary and ten ml flowmeters.

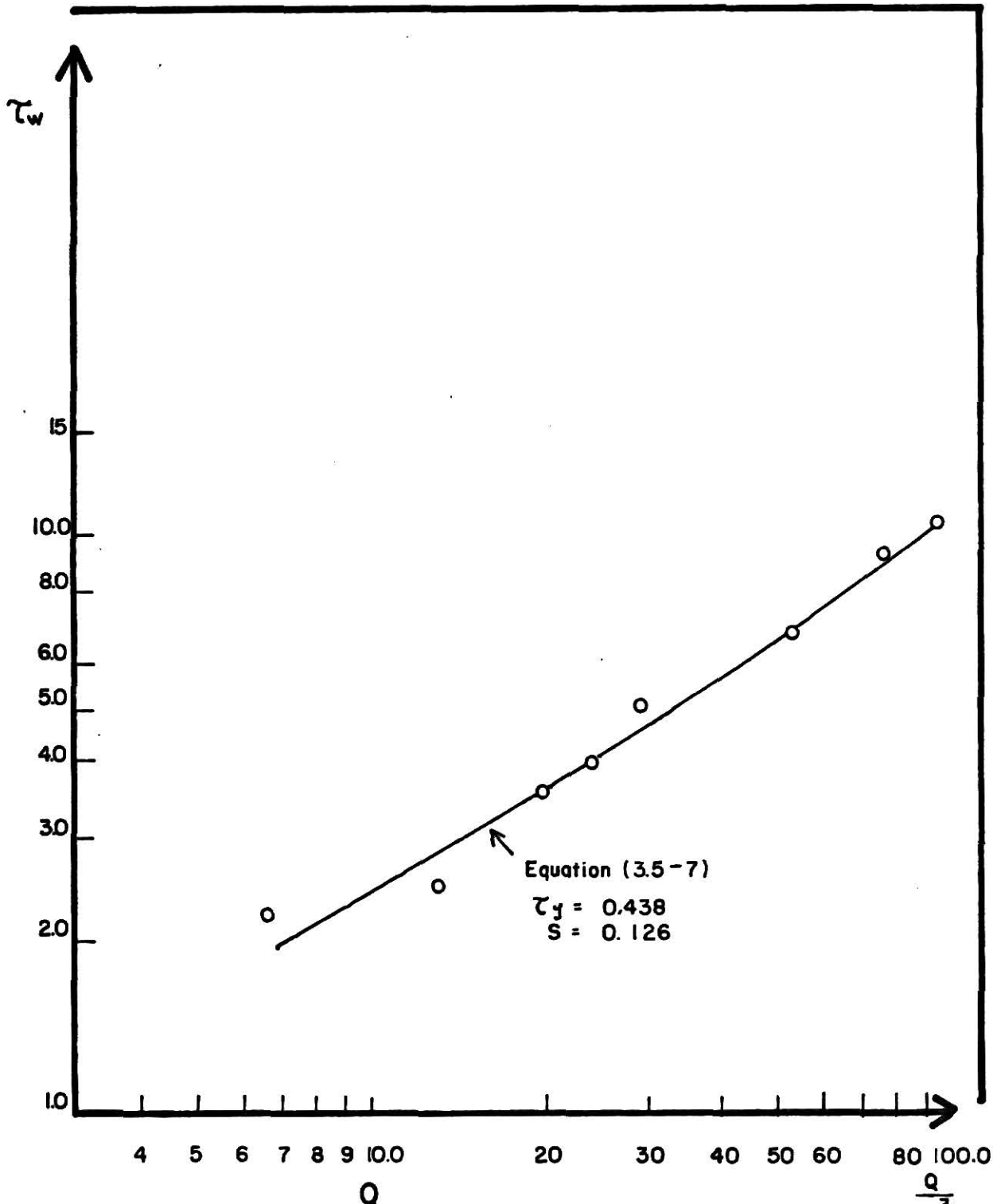

Fig. 14. Plot of τ_w vs $\frac{Q}{\pi R^3}$ for silica suspension concentration of ϕ=0.20 using the 25 ml flowmeters.

The approximate relation:

$$\tau_w = \frac{188}{147}\tau_y + \frac{32S}{7}\tau_y^{1/2}\sqrt{Q/\pi R_c^3} + \frac{4S^2Q}{\pi R_c^3}, \qquad (3.5\text{-}7)$$

which was developed for the Casson fluid in Section 3.5 is indicated by the solid line in these plots. The parameters τ_y and S appearing in the above equation were obtained from $\sqrt{\tau_w}$ versus $\sqrt{\gamma_w}$ plots. As is indicated in the Figures, the experimental data show good agreement with Equation (3.5-7) in the non-Newtonian region.

For $\phi = 0.05$, some of the experimental data appear to deviate from the theoretical equation for $\tau_w < 0.8$. This deviation is expected, because of the Newtonian nature of the flow in this region as indicated previously.

The Casson model appears to be equally applicable to the description of the rheological behavior in the non-Newtonian region.

It may also be of interest to compare the various relations between τ_w and $\bar{U}$ for the Casson fluid which were presented in Section 3.5. Equations (3.5-10), (3.5-11), (3.5-19), (3.5-20), and (3.5-21) were compared for a wide range of $\bar{U}$ (0.001 - 10 sec^{-1}) for both low and high solids concentration. The values of τ_y and S used in these calculations were the experimental values determined from the $\sqrt{\tau_w}$ versus $\sqrt{\gamma_w}$ plots. In Tables 6 and 7 the results of this comparison are presented for low and high solids concentration respectively.

Equations (3.5-11), (3.5-19), and (3.5-20) were in good agreement with the exact Casson Equation (3.5-10) for values of $\bar{U}$ above 0.1 sec. For high values of $\bar{U}$, $\bar{U} > 10$, τ_w values calculated from Equation (3.5-21) deviate from those obtained from the other equations. For lower values of $\bar{U}$ slight

deviations were observed as can be seen from these tables. This is due to the term $(\tau_y/\tau_w)^4$, neglected in Equation (3.5-10) for values of $\tau_y < 0.4\ \tau_w$. At low values of $\bar{U}$ this term becomes important and hence the above variation is observed.

TABLE 6

COMPARISONS BETWEEN τ_w AND $\bar{U}$ FOR ϕ=0.05

τ_w dyne/cm^2

$\bar{U}$ (sec^{-1})	Eq(3.5-10)	Eq(3.5-11)	Eq(3.5-19)	Eq(3.5-20)	Eq(3.5-21)
10.000	0.804	0.804	0.805	0.801	0.814
1.000	0.171	0.171	0.172	0.170	0.172
0.100	0.0661	0.0678	0.0686	0.0675	0.0679
0.010	0.0414	0.0448	0.0456	0.0448	0.0449
0.001	0.0335	0.0385	0.0393	0.0385	0.0386

TABLE 7

COMPARISONS BETWEEN τ_w AND $\bar{U}$ FOR ϕ=0.20

$\bar{U}$ (sec^{-1})	Eq(3.5-10)	Eq(3.5-11)	Eq(3.5-19)	Eq(3.5-20)	Eq(3.5-21)
50.000	10.7	10.7	10.7	10.7	10.9
10.000	3.54	3.54	3.55	3.52	3.56
1.000	1.21	1.23	1.24	1.22	1.23
0.100	0.695	0.743	0.755	0.742	0.744
0.010	0.541	0.615	0.627	0.615	0.616
0.001	0.482	0.577	0.589	0.577	0.578

5.3 Friction Factor Correlation

The experimental data were compared with the friction factor expression for the Casson fluid and the generalized method of Metzner and Reed. The friction factor expression for the Power law fluid was not considered because of the similarity with the generalized method.

Casson fluid. In Figure 15 a typical plot of the friction factor (f) versus modified Reynolds number (R_e^*) is presented for a solids concentration of $\phi = 0.05$.

The experimental values for f and R_e^* were calculated by using Equations (3.6-3) and (3.6-9) respectively which are restated below:

$$f = \frac{2}{\rho R^2} \frac{\tau_w}{\left(\frac{Q}{\pi R^3}\right)^2} , \tag{3.6-3}$$

and

$$R_e^* = \frac{2 R^2 \rho}{S^2} \left(\frac{Q}{\pi R^3}\right) . \tag{3.6-9}$$

The theoretical line obtained from Equation (3.6-8) is also presented in this figure. As can be seen there is agreement between the experimental values and the theoretical line in the non-Newtonian region.

The experimental points corresponding to the Newtonian region, follow the theoretical equation $f = 16/R_e^*$. The experimental points corresponding to the non-Newtonian region deviate from this theoretical line as can be seen in Figure 15. Reynolds numbers for this region were calculated by using Equation (3.6-9) but with the Newtonian viscosity μ in place of S^2.

For high solids concentration, $\phi = 0.20$, only the non-Newtonian region was observed; good agreement with the theoretical Casson expression, Equation (3.6-15) was obtained.

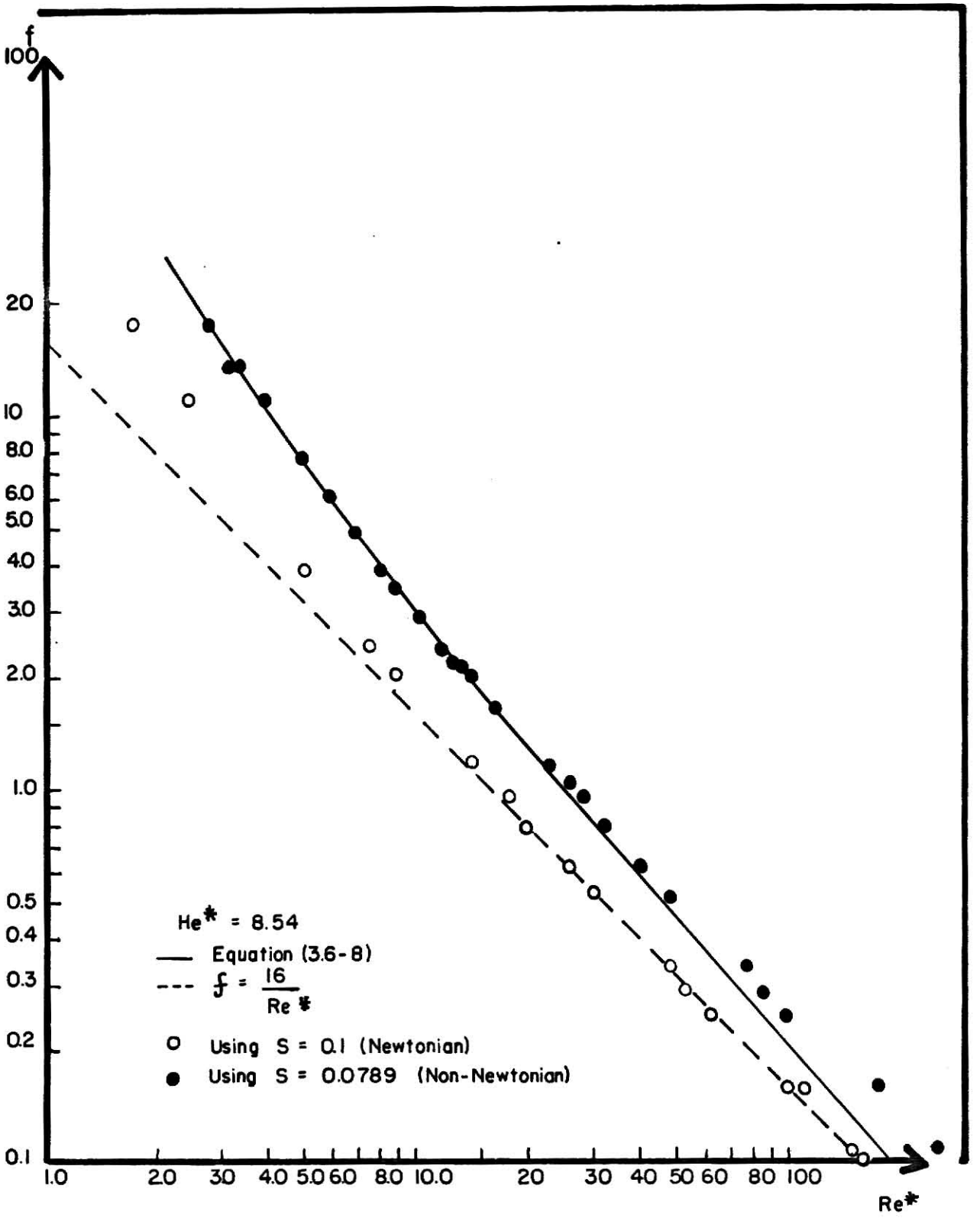

Fig. 15. Friction factor plot using Casson approximate equation for solids concentration of $\phi = 0.05$.

Generalized method of Metzner and Reed. The following procedure was employed for obtaining friction factor plots by this method.

1. Plots of $\log(\tau_w)$ versus $\log(\gamma_w)$ for low and high solids concentration were obtained.

2. Values of n (slope) and k (intercept) were calculated for the linear portions in such plots.

3. Values of n' and k' were calculated from the following equations:

$$n = n' \tag{3.6-19}$$

and

$$k = k' \left(\frac{4n'}{3n' + 1}\right)^{n'} \tag{3.6-20}$$

4. Experimental values of f were calculated by using the same equation as for the Casson fluid. Experimental values of Reynolds numbers were calculated by using Equation (3.6-22), which is restated below;

$$N_{Re} = \frac{D^{n'} U_m^{2-n'} \rho}{8^{n'-1} k'} \tag{3.6-22}$$

where U_m can be obtained from Equation (3.6-14) as:

$$U_m = R\left(\frac{Q}{\pi R^3}\right) \tag{5.3-1}$$

5. The calculated values of friction factors (f) and Reynolds numbers N_{Re} were plotted on a log-log scale.

Figure 16 is the friction factor plot by the method of Metzner and Reed, for both, low and high solids concentration. The experimental values of f and N_{Re} for both Newtonian and non-Newtonian regions were in good agreement with the theoretical equation for laminar flow $f = 16/N_{Re}$.

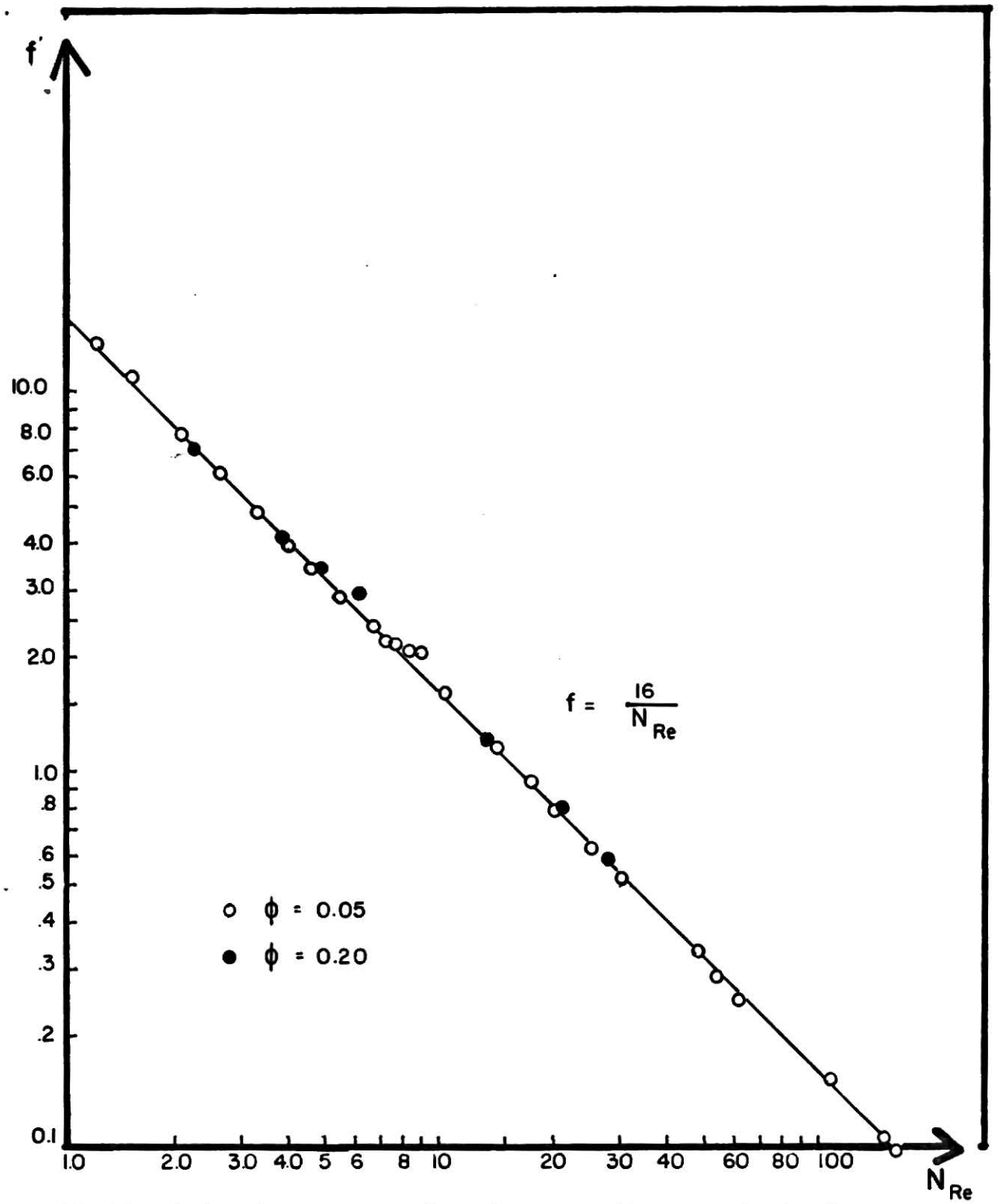

Fig. 16. Friction factor plot using the generalized method of Metzner and Reed. Silica suspension concentration of $\phi = 0.05$ and $\phi = 0.20$.

According to Metzner and Reed (28) the concordance between experimental points in the laminar region and the theoretical equation $f = 16/N_{Re}$, provides a good criteria for the reliability of the data of time-independent fluids.

In addition, Metzner and Reed have considered that any fluid can be described by Power law model over limited regions. In this case, the Reynolds number expressed in terms of the Power law parameters becomes identical to the Reynolds number defined for a Power law fluid. Therefore the method for friction factor using the Power law model is in principle similar to the method by Metzner and Reed and is not necessary to be considered here.

CHAPTER 6

CONCLUSIONS, DISCUSSION AND RECOMMENDATIONS

The conclusions of this study and some discussion concerning the rheological behavior of silica suspensions are presented in this chapter. In addition the approximations to Casson equation and friction factor curves are discussed. Some comments about the instrument and recommended modifications are also included.

The observations of the rheological behavior of silica suspensions indicate that:

1. At low solids concentration and high shear rates, Newtonian behavior is present. In particular for $\phi = 0.05$ the range of Newtonian behavior was for shear rates values of $\gamma_w > 64\ sec^{-1}$.

2. At low solids concentration and low shear rates, non-Newtonian behavior is present. For $\phi = 0.05$ this behavior was observed for shear rates of $\gamma_w > 64\ sec^{-1}$.

3. At high solids concentration, $\phi = 0.20$, non-Newtonian behavior was observed over the entire range of shear investigated.

4. Both, Power law and Casson models described the data well in the non-Newtonian region but not in the Newtonian region.

The physical explanation of the first three observations can be given in the following terms; at rest, the suspension contains a three dimensional structure of sufficient rigidity to resist any stress less than the yield stress τ_y. When a stress greater than τ_y is applied the suspension will flow and the initial structure is broken down into substructure of particles. The behavior observed depends on the intensity of the intraparticle attractive

forces. These groups are subjected to disruptive stresses by the flowing medium, the magnitude of which increases with increasing shear rate. For every shear rate a different viscosity of the suspension is obtained; hence non-Newtonian behavior results. Contrary to thixotropic behavior the change in structure with changes in shear take place so fast that no dependence on time is observed. At higher shear rates a condition is reached in which the structure or groups of particles no longer breaks down. The viscosity of the suspension remains constant with further increase in shear rate. This is the region of Newtonian behavior.

It may also be of interest to compare the results obtained in the present investigation with those obtained by Merril and coworkers (26) for human blood. The following similarities between silica suspensions and blood flow have been observed:

1. Newtonian behavior is observed in both, at sufficiently high shear rates.

2. At lower shear rates both can be described by the Casson and Power law models over the appropriate range of shear rates.

3. A transition region from Newtonian to non-Newtonian flow is observed in both of them. However, the characteristics are different for each fluid.

In Figure 17 a qualitative comparison of the transition regions obtained by Merril and that obtained in the present investigation is shown in the form of square root coordinates. The transition region obtained by Merril and coworkers is represented by a smooth curve which separates the Newtonian and the non-Newtonian regions. The special feature of this plot is that the line describing non-Newtonian behavior has approximately the same slope to that obtained for the Newtonian region. In the present work, an abrupt change from

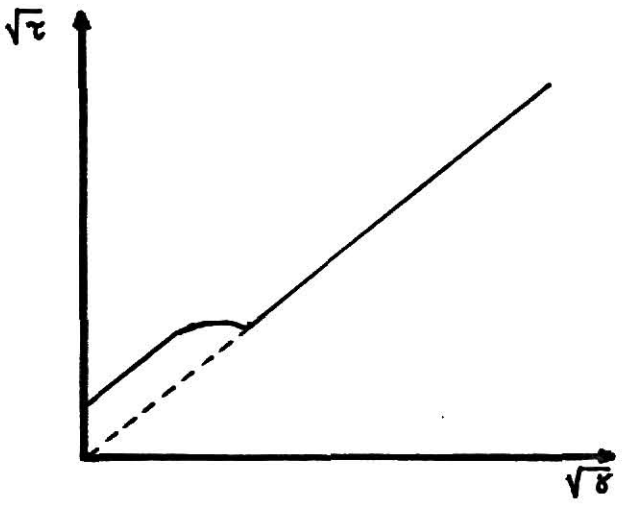

Transition region for blood flow obtained by Merrill and Coworkers.

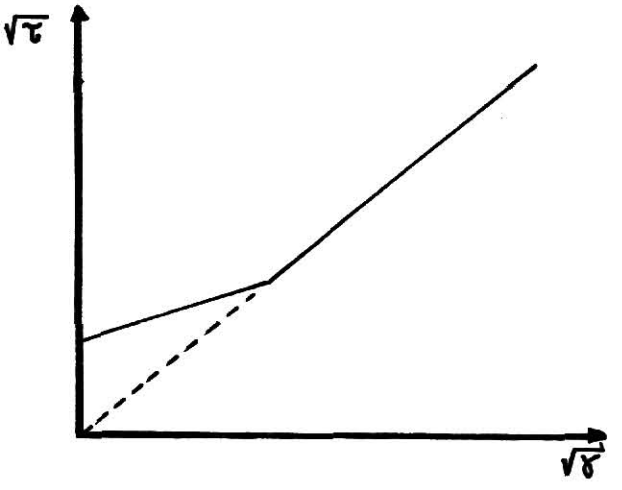

Transition region for silica suspension concentration of $\theta = 0.05$.

Fig. 17. Comparisons between transition regions for blood and silica suspensions.

Newtonian to non-Newtonian behavior was observed with silica suspension (concentration of $\phi = 0.05$). The slope of the line describing non-Newtonian behavior was substantially different from that obtained in the Newtonian region.

On the basis of the above comparisons, it is suggested that silica suspension may be a good test fluid for model blood flow studies.

It may be also of interest to present some discussion concerning the various approximations to Casson equation considered in Chapters 3 and 5. For convenience to the reader these equations are restated in Table 8. The approximate Equation (3.5-7), relating the wall shear stress τ_w and the reduced average velocity $Q/\pi R^3$, was in very good agreement (as indicated by numerical comparison) with the exact Casson equation, Equation (3.5-4). It was also in good agreement with the experimental data in the non-Newtonian region, as indicated in Figures 13 and 14.

For low values of $Q/\pi R^3$, or $\bar{U}$ (see Tables 6 and 7) Equation (3.5-7) deviates from the exact Casson equation. This deviation is due to the condition imposed on Equation (3.5-4), that $\tau_y/\tau_w < 0.4$. This condition is no longer satisfied at low values of $Q/\pi R^3$ and hence the deviation occurs. The magnitude of $Q/\pi R^3$ below which this condition is no longer satisfied depends on the parameters τ_y and S. As can be seen from Figure 13, the experimental data of this study deviate considerably from the Casson equation in the Newtonian region, indicating that this equation is not applicable in this region. This deviation would be expected on the basis of the results presented in Figure 11 which indicate that the square of the Casson viscosity S^2 is different from the Newtonian viscosity μ. Hence the Casson equation would not be expected to describe the data in the Newtonian region.

TABLE 8

APPROXIMATE CASSON EQUATIONS

No.	Equation
(3.5-4)	$Q/\pi R^3 = \frac{\tau_w}{S^2}\left[\frac{1}{4} + \frac{1}{3}\left(\frac{\tau_y}{\tau_w}\right) - \frac{4}{7}\left(\frac{\tau_y}{\tau_w}\right)^{1/2} - \frac{1}{84}\left(\frac{\tau_y}{\tau_w}\right)^4\right]$
(3.5-7)	$\tau_w = \frac{188}{147}\tau_y + \frac{32S}{7}\tau_y^{1/2}\sqrt{\frac{Q}{\pi R^3}} + 4S^2\frac{Q}{\pi R^3}$
(3.5-11)	$\tau_w = \frac{188}{147}\tau_y + \frac{32\sqrt{2}\,S}{7}\tau_y^{1/2}\sqrt{\bar{U}} + 8S^2\bar{U}$
(3.5-12)	$\tau_w^{1/2} = \tau_y^{1/2} + S\,\gamma_w^{1/2}$
(3.5-15)	$\tau_w^{1/2} = \tau_y^{1/2} + 2\sqrt{2}\,S\,\bar{U}^{1/2}$
(3.5-16)	$\tau_w = \tau_y + 4\sqrt{2}\,S\,\tau_y^{1/2}\sqrt{\bar{U}} + 8\,S^2\,\bar{U}$
(3.5-19)	$\tau_w^{1/2} = 1.143\,\tau_y^{1/2} + 2\sqrt{2}\,S\,\bar{U}^{1/2}$
(3.5-20)	$\tau_w^{1/2} = 1.131\,\tau_y^{1/2} + 2\sqrt{2}\,S\,\bar{U}^{1/2}$
(3.5-21)	$\tau_w^{1/2} = 1.131\,\tau_y^{1/2} + 2.021\sqrt{2}\,S\,\bar{U}^{1/2}$

In contrast, Merril and coworkers (26) observed from blood flow data that the square of the Casson viscosity was approximately the same as the Newtonian viscosity. In this case the Casson model can be extended to the Newtonian region with negligible error. The applicability of the Casson equation to the Newtonian region has been observed by several other workers (38).

Numerical comparisons between Equation (3.5-7) and Merril's approximate Equation (3.5-16) expressed in terms of $Q/\pi R^3$, were made. It was found that Equation (3.5-7) provides a better description than the approximation of Merril and coworkers for blood flow data.

The three approximate relations between $\sqrt{\tau_w}$ and $\sqrt{\bar{U}}$, equations (3.5-19), (3.5-20), and (3.5-21) when squared provide reasonable approximation to Equation (3.5-11). These equations and also the exact Casson equation, Equation (3.5-10), were compared numerically for a wide range of $\bar{U}$ values. The results are presented in Tables 6 and 7. For low values of $\bar{U}$ (dependent on the magnitude of τ_y and S) deviations between the approximate equations and the exact equation were observed. These are due to the fact that $\tau_y/\tau_w < 0.4$. For high values of $\bar{U}$ the approximation from Equation (3.5-21) also showed a deviation from the exact Casson equation. This was due to the error in leading term. For this reason, Equation (3.5-21) is not suggested as good approximation. The remaining forms obtained, Equations (3.5-19) and (3.5-20), were in good agreement with the exact Casson equation and with the approximation (3.5-11), provided that $\tau_y/\tau_w < 0.4$. Equation (3.5-19) predicted slightly higher values of τ_w whereas Equation (3.5-20) predicted slightly lower values of τ_w. However both equations can be considered to be reasonable approximations.

Since it is much easier to evaluate $\bar{U}$ than γ_w from experimental data these relations offer the advantage of providing a simple method for the evaluation of the Casson parameters $\sqrt{\tau_y}$ and S (from $\sqrt{\tau_y}$ versus $\sqrt{\bar{U}}$ plots). A similar expression relating the $\sqrt{\tau_w}$ and $\sqrt{\bar{U}}$ was given by Merril and coworkers [see Equation (3.5-15)]. This equation was formulated on the basis of the assumption that N ($N = \frac{d \ln \bar{U}}{d \ln \tau_w}$) can be considered constant over limited ranges of τ_w. Merril and coworkers arbitrarily setted N = 1 (the case of Newtonian behavior).

With this assumption, identical values of $\sqrt{\tau_y}$ will be obtained from $\sqrt{\tau_w}$ versus $\sqrt{\bar{U}}$ and $\sqrt{\tau_w}$ versus $\sqrt{\gamma_w}$ plots. This is illustrated by comparison of Equation (3.5-15) and Equation (3.5-12). Their equation also provided a good description of blood flow data and extrapolated data showed the same intercept on the $\sqrt{\tau_w}$ axis.

On the other hand Equations (3.5-19) and (3.5-20) provided a better description of the data obtained in the present investigation. In this case intercepts obtained from $\sqrt{\tau_w}$ versus $\sqrt{\bar{U}}$ and $\sqrt{\tau_w}$ versus $\sqrt{\tau_w}$ plots, were not the same. This would be expected on the basis of a comparison of Equations (3.5-19) and (3.5-20) with Equation (3.5-12). Recall, that the former equations were obtained from the exact Casson equation by approximations based only on order of magnitude considerations in contrast to the somewhat questionable assumption of Merril and coworkers. On this basis, the approximations developed here appear to be more reasonable than Merril's approximation.

The generalized method of Metzner and Reed, for the correlation of friction factor data and the method developed in this study for a Casson fluid both described the experimental data of the present investigation. The

latter was not valid for the Newtonian region. As discussed in Chapter 5 the method of Metzner and Reed offers the particular feature of providing an indication of the accuracy of both Newtonian and non-Newtonian experimental data for the laminar flow region. The friction factor correlation for a Casson fluid also provided a good criteria for the accuracy of the experimental data in the non-Newtonian region. By using this method, the presence of Newtonian behavior is indicated by the deviation of the experimental data from the theoretical friction factor curve. This behavior is illustrated in Figure 15.

When a fluid is known to follow Casson behavior, a minimum of two measurements of shear stress and volumetric flow rate (to evaluate $\bar{U}$) are required to evaluate the Casson parameters τ_y and S. With this information pressure drops in tube flow can be predicted by using either the expression for pressure drop [Equation (3.5-8)], or, the corresponding friction factor versus Reynolds number curve for the appropriate modified Hedström number. Either of the above procedures should offer some advantage over the generalized method by Metzner and Reed which requires a more extensive treatment of the data to evaluate the pressure drop.

However, if friction factor methods are to be compared with pressure flow theoretical expressions for the prediction of pressure drops in pipelines transporting a particular non-Newtonian fluid (i.e. Power or Casson fluid), Harris and Quader (13) have recently pointed out that rearranging data in the form of friction factor correlations offer no special advantage to the designer and in general makes experimental data more inaccessible. The correlation does provide a method for the comparison of data, however for the purpose of design it is probably best to employ the pressure flow relation

directly when the flow behavior is known.

The viscometer and the methods developed in this investigation have several desirable features. These are summarized as follows:

1. The apparatus is simple in both construction and operation.

2. The cost is relatively low.

3. The calibration is straightforward.

4. Settling of suspensions can be readily detected if overlapping data are employed in the measurements. When slopes m of $\log(\Delta P_m - \rho gh)$ versus t plots were compared at same values of wall shear stress τ_w, it was found that they had identical values for flow times less than 200 sec. For higher intervals of flow times these slopes were greater in absolute value indicating that settling was present.

5. The data analysis is simple and reliable. At high shear rate the $\log(\Delta P_m - \rho gh)$ versus t plots are straight lines, the slope m is directly determined and wall shear rates can easily be calculated from Equation (5.1-2). If they are not straight lines (low shear rates) slopes are determined at several selected points and the corresponding wall shear rates are calculated from Equation (3.4-19).

Although this instrument is similar in construction to the instrument described by Benis (2), the method of operation and analysis is considerably different. The unsteady state method of operation employed in this study provides data that are considerably more consistent and reliable over a much wider range of shear than can be obtained by the quasisteady state method used by Benis.

The construction of the instrument is not entirely suitable for high shear measurements with suspensions of low consistency. For example it was

observed for $\phi = 0.05$ that the maximum applied pressure that can be employed was 30 cm of Hg. Applied pressures of this magnitude and higher resulted in significant pressure losses which are not attributable to the capillary alone. This situation was indicated by the calibration data with distilled water which resulted in non-linear $\log(\Delta P_m - \rho gh)$ versus t plots for $\Delta P_m > 30$ Hg. The main reason for this deviation was the inertial pressure losses in the connectors, resulting from the high flow and the abrupt expansions and contractions in this region. Further work can be geared towards resolving this difficulty. Proper design of the connectors should help to eliminate this problem.

Other minor difficulties with the instrument employed in these studies can be resolved with a minimum of effort. Some suggestions are listed below.

1. Changes in pressure when stopcock 2 is opened can be reduced by using a larger air chamber.

2. Since some settling problems arise in the instrument when high solids concentration suspension are employed, the following change is recommended. A syringe connected to the by-pass tube can be employed for mixing the suspension in between runs. This should provide a good agitation and hence a good mix prior to each run. In this way the need for repeats of data because of settling can be avoided.

3. A polynomial approach was employed in the curve fittings to describe both the $\log(\Delta P_m - \rho gh)$ versus t and the h^* versus t data. With the former data the polynomial relationships provided a good value for the slopes m as indicated by comparison with graphically determined values. However, reasonable values of the second derivatives (dm/dt) could not always be obtained from these polynomials. This was indicated by comparison with graphical

evaluations of the second derivatives. With the latter, the polynomial relations did not give reasonable initial values of h^*.

On the basis of the above mentioned difficulties further work should be conducted to find a better functional relationship for the description of the data.

NOMENCLATURE

A cross section area, cm^2.

a constant in Equation (2.16b), dimensionless.

B instrument physical parameters, $cm^2\ sec^{-2}$.

b intercept from a $\sqrt{\tau_w}$ vs $\sqrt{\bar{U}}$ plot, $gm^{1/2}\ cm^{-1/2}\ sec^{-1}$.

C concentration in weight per unit volume, $gm\ cm^{-3}$.

c integration constant in Equation (3.4-14), dimensionless.

D tube diameter, cm.

D_p particle diameter, cm.

f friction factor, dimensionless.

g gravity acceleration, $cm\ sec^{-2}$.

H variable in Equation (5.1-13), dimensionless.

H_e^* modified Hedström number, dimensionless.

h total difference between flowmeter meniscii, cm.

h^* mensicus height in one flowmeter, cm.

k power law parameter, $gm\ cm^{-1}\ sec^{-n}$.

k_0 Casson parameter, $gm^{1/2}\ cm^{-1/2}\ sec^{-1}$.

k_1 Casson parameter, $gm^{1/2}\ cm^{-1/2}\ sec^{-1/2}$.

k' constant defined in Equation (3.6-15), $gm\ cm^{-1}\ sec^{n'-2}$.

L capillary length, cm.

m slope defined in Equation (3.4-16), sec^{-1}.

m' slope obtained from a $\sqrt{\tau_w}$ versus $\sqrt{\bar{U}}$ plot, $gm^{1/2}\ cm^{-1/2}\ sec^{-1/2}$.

N factor defined in Equation (3.5-13), dimensionless.

N_{Re} generalized Reynolds number defined in Equation (3.6-22), dimensionless.

n power law parameter, dimensionless.

n' variable defined in Equation (3.6-12), dimensionless.

Q volumetric flow rate, $cm^3\ sec^{-1}$.

R constant radius, cm.

R_{b1} LSH flowmeter tube radius, cm.

R_{b2} RHS flowmeter tube radius, cm.

R_c capillary radius, cm.

R_F flowmeter radius, cm.

R'_e Power law modified Reynolds number defined in Equation (3.6-7), dimensionless.

R^*_e Casson model modified Reynolds number defined in Equation (3.6-9), dimensionless.

r variable radius, cm.

S Casson viscosity, $gm^{1/2}\ cm^{-1/2}\ sec^{-1/2}$.

s' relative sediment volume, dimensionless.

t time, sec.

$\bar{U}$ relative average fluid velocity, sec^{-1}.

U_m average flow velocity cm sec^{-1}.

u variable velocity, cm sec^{-1}.

v_r radial velocity, cm sec^{-1}.

v_θ tangential velocity, cm sec^{-1}.

x distance, cm.

x_o equilibrium distance, cm.

y distance, cm.

y_o equilibrium distance, cm.

GREEK LETTERS

α constant in Equation (2.16b), dimensionless.

β constant in Equation (2.16b), dimensionless.

γ shear rate, sec^{-1}.

γ_w wall shear rate, sec^{-1}.

$\tilde{\Delta}$ rate of deformation tensor.

ΔF correction factor defined by Equation (3.3-8), dimensionless.

ΔP applied pressure across the capillary, dyne cm^{-2}.

ΔP_m applied pressure to the LHS flowmeter, dyne cm^{-2}.

δ variable defined by Equation (5.1-4), dimensionless.

η apparent viscosity, gm cm^{-1} sec^{-1}.

η_a effective viscosity, gm cm^{-1} sec^{-1}.

η_{rel} relative viscosity, dimensionless.

η_{sp} specific viscosity, dimensionless.

θ constant in Equation (2.1-7), dyne cm^{-2}.

K voluminosity factor, dimensionless.

μ Newtonian viscosity, gm cm^{-1} sec^{-1}.

μ_o viscosity of the suspending medium, gm cm^{-1} sec^{-1}.

ρ density, gm cm^{-3}.

ρ_p particle density, gm cm^{-3}.

$\tilde{\tau}$ viscous tensor.

τ shear stress, dyne cm^{-2}.

τ_{rz} shear stress in the z direction, dyne cm^{-2}.

τ_y yield stress, dyne cm^{-2}.

τ_w wall shear stress, dyne cm^{-2}.

ϕ volume fraction of solids, dimensionless

ϕ_a effective fluidity, gm^{-1} cm sec.

ϕ_∞ volume fraction of solids for infinite viscosity, dimensionless.

ACKNOWLEDGMENTS

The author wishes to express his sincere gratitude to his major advisor, Dr. W. P. Walawender under whose direction this work was carried out, for his guidance and constant help.

The author also wishes to express his gratitude to Dr. L. T. Fan for his help in obtaining financial support.

REFERENCES

1. Aris, R., "Vectors, Tensors, and the Basic Equations of Fluid Mechanics," Prentice Hall, Inc., Englewood Cliffs, N. J. (1962).

2. Benis, A. M., "A New Simple Low Shear Capillary Viscometer for Blood," Biorheology, 5 (1968), pp. 263-270.

3. Bird, R. B., Stewart, W. E., Lightfoot, E. N., "Transport Phenomena," John Wiley and Sons, Inc., New York (1960).

4. Caraher, J. M., "An Ultra-Low Shear Rate Viscosimeter," Symposium on Rheology, The American Society of Mechanical Engineers, ed. by A. W. Marris and J. T. S. Wang.

5. Casson, N., "Rheology of Disperse Systems," ed. C. C. Mill, Pergamon Press, London (1959), pp. 84-104.

6. Cerny, L. C., Cook, F. B., and Walker, C. C., "Rheology of Blood," American Journal of Physiology, 6 (1962), pp. 1188-1194.

7. Charm, S., and Kurland, G. S., "Tube Flow Behavior and Shear Stress-Shear Rate Characteristics of Canine Blood," American Journal of Physiology, 203 (1962), pp. 417-421.

8. Dodge, D. W., and Metzner, A. B., "Turbulent Flow of Non-Newtonian System," A.I.Ch.E. Journal, 5, No. 2 (June, 1959), pp. 189-204.

9. Ford, T. F., "Viscosity Concentration and Fluidity Concentration Relationships for Suspensions of Spherical Particles in Newtonian Liquids," Journal of Physics and Colloid Chemistry, 64 (Sept., 1960), pp. 1168-1174.

10. Frisch, H. L., Simha, R., Ed. Eirich, F. R., "Rheology, Theory and Applications," Vol. 1, Academic Press, Inc., New York (1956).

11. Gay, E. C., and Nelson, P. A., "Flow Properties of Suspensions with High Solids Concentration," A.I.Ch.E. Journal, 15, No. 6 (Nov., 1969), pp. 815-822.

12. Gay, E. C., Ph.D. thesis, Washington University. St. Louis, Mo. (1967).

13. Harris, J., and Quader, A. K. M. A., "Design Procedures for Pipelines Transporting Non-Newtonian Fluids and Solid-Liquid Systems," British Chemical Engineering, 16, No. 4/5 (May, 1971), pp. 307-311.

14. Hedström, B. O. A., Industrial Engineering Chemistry (1952), 44, 651.

15. Hershey, D., and Cho, S. J., "Blood Flow in Rigid Tubes: Thickness and Slip Velocity of Plasma Film at the Wall," Journal of Applied Physiology, 21 (1966), pp. 27-32.

16. Hershey, D., and Gupta, B. P., "The Effect of Tube Diameter on the Laminar Regime Transition for a Non-Newtonian Suspension (Blood)," Biorheology, 5 (1968), pp. 313-321.

17. Kenny, J. P., Wasp, E. J., and Thompson, T. L., "A Design Model for Pipeline Flow of Solid Wastes," Federal Water Pollution Control Administration of the Department of the Interior, Contract No. 14-12-156.

18. Hershey, D., and Smolin, R., "Laminar Regime Transition for Blood Flow in Tubes," Biorheology, 4 (1967), pp. 61-67.

19. Krieger, I. M., and Elrod, H., "Direct Determination of the Flow Curves of Non-Newtonian Fluids. II. Shearing Rate in the Concentric Cylinder Viscometer," Journal of Applied Physics, 24, No. 2 (Feb., 1953), pp. 134-136.

20. Krieger, I. M., and Maron, S. H., "Direct Determination of the Flow Curves of Non-Newtonian Fluids. III. Standardized Treatment of Viscometric Data," Journal of Applied Physics, 25, No. 1 (Jan., 1954), pp. 72-75.

21. Krieger, I. M., and Maron, S. H., "Direct Determination of the Flow Curves of Non-Newtonian Fluids," Journal of Applied Physics, 23, No. 1 (Jan., 1952), pp. 147-149.

22. Maron, S. H., and Belner, R. J., "Low Shear Capillary Viscometer with Continuously Varying Pressure Head," Journal of Applied Physics, 26, No. 12 (Dec., 1955), pp. 1457-1460.

23. Maron, S. H., Krieger, I. M., and Sisko, A. W., "A Capillary Viscometer with Continuously Varying Pressure Head," Journal of Applied Physics, 25, No. 8 (Aug., 1954), pp. 971-975.

24. McDermott, W. F., Cowper, N. T., David, R. A., and Wasp, E. J., "The World's First Long Distance Iron Ore Slurry Pipeline," Soc. Min. Eng. of AIME, Minneapolis, Minnesota (Sept., 1968).

25. Merril, E. W., Benis, A. M., Gilliland, E. R., Sherwood, T. K., and Salzman, E. W., "Pressure-Flow Relations of Human Blood in Hollow Fibers at Low Flow Rates," Journal of Applied Physiology, 20 (1965), pp. 954-967.

26. Merril, E. W., and Pelletier, G. A., "Viscosity of Human Blood: Transition from Newtonian to Non-Newtonian," Journal of Applied Physiology, 23 (1967), pp. 178-182.

27. Metzner, A. B., "Non-Newtonian Fluid Flow," Industrial and Engineering Chemistry, 49, No. 9 (Sept., 1957), pp. 1429-1432.

28. Metzner, A. B., and Reed, J. C., "Flow of Non-Newtonian Fluids--Correlation of the Laminar, Transition, and Turbulent-flow Regions," A.I.Ch.E. Journal, 1, 434 (Dec., 1955), pp. 434-440.

29. Mill, C. C. (ed.), "Rheology of Disperse Systems," Pergamon Press, Oxford (1959).

30. Mishra, P. N., Severson, D. E., and Owens, T. C., "Rheological Study of Concentrated Silica Suspensions," Chemical Engineering Science, 25 (1970), pp. 653-663.

31. Mishra, P. N., "Rheological Study of Concentrated Silica Suspensions," University of North Dakota, M. S. Thesis (1969).

32. Mooney, M., "The Viscosity of a Concentrated Suspension of Spherical Particles," Journal of Colloid Science, 6 (1951), pp. 162-170.

33. Mooney, M. J., Rheology, 2 (1931), p. 210.

34. Moreland, C., "Viscosity of Suspensions of Coal in Mineral Oil," The Canadian Journal of Chemical Engineering (Feb., 1963), pp. 24-28.

35. Oka, S., "An Approach to a Unified Theory of the Flow Behavior of Time-Independent Non-Newtonian Suspensions," Japanese Journal of Applied Physics, 10, No. 3 (March, 1971), pp. 287-291.

36. Rabinowitsch, B. Z., Phys. Chem. (1939), A 145 1.

37. Scott Blair, G. W., "Elementary Rheology," Academic Press, London (1969), Chap. 8, pp. 45-49.

38. Scott Blair, G. W., "An Equation for the Flow of Blood, Plasma and Serum Through Glass Capillaries," Nature, 183, No. 461 (1959), pp. 613-614.

39. Sharp, A. N., "Coal by Pipeline," Coke and Gas (Aug., 1961), pp. 336-338.

40. Skelland, A. H. P., "Non-Newtonian Flow and Heat Transfer," John Wiley and Sons, Inc., New York (1967).

41. Tamamushi, B. I., "Empirical Relations and Structural Models for Blood Flow," Biorheology, 6 (1970), pp. 235-236.

42. Thomas, D. G., "Non-Newtonian Suspensions: Part I: Physical Properties and Laminar Transport Characteristics," Industrial Engineering Chemistry, 55, No. 11 (Nov., 1963), pp. 18-29.

43. Ting, A. P., Luebbers, R. H., "Viscosity of Suspensions of Spherical and Other Isodimensional Particles in Liquids," A.I.Ch.E. Journal, 3, No. 1 (1957), pp. 111-116.

44. Vand, V., "Viscosity of Solutions and Suspensions, II," Journal of Physics and Colloid Chemistry, 52 (1948), pp. 300-314.

45. Van Wazer, J. R., Lyons, J. W., and Kim, K. Y., "Viscosity and Flow Measurements. A Laboratory Handbook of Rheology," Interscience Publishers, a division of John Wiley and Sons (1963).

46. Walawender, W. P., personal communication.

47. Walker, J. R. D., and Worster, R. C., "Hydraulic Transport of Solids-Trinidad Cement Ltd.'s 6-mile, 2000 psi Pipeline," The Pipes, Pipelines, Pumps and Valves Convection, Earls Court, London (April, 1962).

48. Wasp, E. J., "Cross Country Coal Pipeline Hydraulics," Pipeline News (July, 1963), pp. 20-28.

49. Weisman, J., "Minimum Power Requirements for Slurry Transport," A.I.Ch.E. Journal, 9, No. 1 (Jan., 1963).

50. Whitmore, R. L., "Rheology of the Circulation," Pergamon Press (1968).

51. Wilkinson, W. L., "Non-Newtonian Fluids," Pergamon Press (1960).

52. Wu, K. E., "The Determination of Parameters in Rheological Models of Silica Suspension in Water," University of North Dakota, M. S. Thesis (1970).

APPENDIX A

Chemical and Physical Characteristics of Silica

TABLE 9

CHEMICAL ANALYSIS (TYPICAL) OF SILICA ( )

Item	IMSIL A-15	IMSIL A-10
Silica (SiO_2)	99.0%	99.0%
Iron Oxide (Fe_2O_3)	0.025%	0.025%
Titanium Oxide (TiO_2)	0.005%	0.005%
Aluminium Oxide (Al_2O_3)	0.009%	0.009%
Calcium Oxide (CaO)	0.15%	0.15%
Magnesium Oxide (MgO)	0.008%	0.008%
Loss on Ignition	0.30%	0.30%

TABLE 10

PARTICLE SIZE DISTRIBUTION FOR SILICA ( )

Particle Size	Grade IMSIL A-15	Grade IMSIL A-10
40 Micron Diameter, Below	100.0%	100.0%
20 Micron Diameter, Below	100.0%	100.0%
15 Micron Diameter, Below	99.0%	100.0%
10 Micron Diameter, Below	96.0%	99.0%
7.5 Micron Diameter, Below	87.0%	91.0%
5.0 Micron Diameter, Below	70.0%	76.0%
Average Particle Size (Fisher Sub-Sieve)	1.82	1.55

TABLE 11

PHYSICAL CHARACTERISTICS (TYPICAL) OF SILICA ( )

Item	IMSIL A-15	IMSIL A-10
Specific Gravity	2.65	2.65
Weight per Solid Gallon, LBS	22.07	22.07
pH value	7	7
Moisture limit at 105°C	0.25%	0.25%
Molecular Weight	60.09	60.09
Melting Point	1722°C	1722°C
Specific Surface Area cm^2/g	12440	14607

APPENDIX B

Least Squares Computer Program

```
340003200701360003200702490240251196361130010 2     MONITOR COLD START
77JOB
77XEQ FORUN
C  C  POLYNOMIAL CURVE FITTING USING LEAST SQUARES  FILE 7.0.002
      DIMENSION X(100),Y(100),A(16,16),SUMX(31),SUMY(15),W(100)
  105 FORMAT(I10,F10.5,I10)
  200 FORMAT(2F10.5)
  300 FORMAT(F12.6,5X,F12.6,5X,F12.6,5X,I3)
  400 FORMAT(E14.6,5X,E14.6)
  500 FORMAT(E14.6,5X,E14.6,5X,E14.6,5X,E14.6)
    1 READ 105,N,TOL,LAST
C     N=NUMBER OF DATA SETS (X AND Y )
C     TOL = ALLOWABLE ERROR
C     LAST = GREATEST ORDER OF FIT
      IF(SENSE SWITCH 1)30,20
C     SENSE SWITCH 1 ON FOR WEIGHTED OBSERVATIONS, OFF FOR NO WEIGHTING
   20 READ 200,(X(I),Y(I),I=1,N)
      GO TO 40
   30 READ,(X(I),Y(I),W(I),I=1,N)
   40 CONTINUE
      IF(SENSE SWITCH 1)70,50
   50 DO 60 I=1,N
   60 W(I)=1.
   70 SUMX(1)=0.
      SUMX(2)=0.
      SUMX(3)=0.
      SUMY(1)=0.
      SUMY(2)=0.
      DO 90 I=1,N
      SUMX(1)=SUMX(1)+W(I)
      SUMX(2)=SUMX(2)+W(I)*X(I)
      SUMX(3)=SUMY(3)+W(I)*X(I)*X(I)
      SUMY(1)=SUMY(1)+W(I)*Y(I)
   90 SUMY(2)=SUMY(2)+W(I)*X(I)*Y(I)
      NORD=1
   91 IF(SENSE SWITCH 4)92,93
C     SENSE SWITCH 4 OFF
   92 ACCEPT,TOL,LAST
   93 L=NORD+1
      KK=L+1
      DO 101 I=1,L
      DO 100 J=1,L
      IK=J-1+I
  100 A(I,J)=SUMX(IK)
  101 A(I,KK)=SUMY(I)
      DO 140 I=1,L
      A(KK,I)=-1.
      KKK=I+1
      DO 110 J=KKK,KK
  110 A(KK,J)=0.
      C=1./A(1,I)
      DO 120 II=2,KK
      DO 120 J=KKK,KK
  120 A(II,J)=A(II,J)-A(1,J)*A(II,I)*C
```

```
      DO 140 II=1,L
      DO 140 J=KKK,KK
  140 A(II,J)=A(II+1,J)
      S2=0.
      DO 160 J=1,N
      S1=0.
      S1=S1+A(1,KK)
      DO 150 I=1,NORD
  150 S1=S1+A(I+1,KK)*X(J)**I
  160 S2=S2+(S1-Y(J))*(S1-Y(J))
      B=N-L
      S2=(S2/B)**.5
      IF(SENSE SWITCH 2)163,161
C     SENSE SWITCH 2 ON
  161 IF(NORD-LAST)162,163,162
  162 IF(S2-TOL)163,163,171
  163 CONTINUE
      PUNCH 300,NORD,TOL,S2,N
      DO 164 I=1,L
      J=I-1
  164 PUNCH 400,J,A(I,KK)
      IF(SENSE SWITCH 3)167,165
C     SENSE SWITCH 3 ON PRINTS EACH FIT
  165 IF(NORD-LAST)166,167,166
  166 IF(S2-TOL)167,167,171
  167 DO 169 I=1,N
      S1=0.
      S1=A(1,KK)
      DO 168 J=1,NORD
  168 S1=S1+A(J+1,KK)*X(I)**J
      S3=Y(I)-S1
  169 PUNCH 500,X(I),Y(I),S1,S2
      IF(NORD-LAST)170,173,173
  170 IF(S2-TOL)173,173,171
  171 NORD=NORD+1
      J=2*NORD
      SUMX(J)=0.
      SUMX(J+1)=0.
      SUMY(NORD+1)=0.
      DO 172 I=1,N
      KKK=J-1
      SUMX(J)=SUMX(J)+X(I)**KKK*W(I)
      SUMX(J+1)=SUMX(J+1)+X(I)**J*W(I)
  172 SUMY(NORD+1)=SUMY(NORD+1)+Y(I)*X(I)**NORD*W(I)
      GO TO 91
  173 PAUSE
      IF(SENSE SWITCH 4)171,1
      END
YYWW
```

DETERMINATION OF RHEOLOGICAL DATA OF SILICA SUSPENSIONS WITH A CAPILLARY VISCOMETER

by

DAVID F. CALA

B. S. (Chem. Eng.), Universidad Industrial de Santander, 1968
M. S. (Mathematics), Kansas State Teachers College, 1969

AN ABSTRACT OF A MASTER'S THESIS

submitted in partial fulfillment of the

requirements for the degree

MASTER OF SCIENCE

Department of Chemical Engineering

KANSAS STATE UNIVERSITY
Manhattan, Kansas

1971

Silica suspension rheological data (shear stress and shear rate) were obtained with a capillary viscometer similar to the one recently described by Benis.

The experimental data were examined for fit to both the Power law and the Casson models. With suspensions of low solids concentration both Newtonian and non-Newtonian behavior was observed at high and low shear rates respectively. Only non-Newtonian behavior was observed with high solids concentration over the limited range of shear investigated. The Casson and Power law models appear to be suitable for the description of the data in the non-Newtonian region.

The capillary viscometer employed in this investigation appears to possess some definite advantages over other types of viscometers employed in the study of suspensions rheology. An unsteady state mode of operation was employed and appears to be superior to the quasi steady state mode of operation proposed by Benis.

An approximate pressure flow relationship for a Casson fluid was examined. This relation was also expressed in terms of the friction factor for comparison with the experimental data. Flow data were also compared with the generalized friction factor correlation of Metzner and Reed. In addition, some approximations to the Casson model were examined.